Highlights

Brines involved in Proterozoic U deposits (Athabasca, Canada) are targeted.

Halogens (Cl, Br, I) indicate a subaerial evaporation of seawater origin for brines.

Brines acquired excess noble gases (Ar, Kr, Xe) by interaction with clastic sediments.

Interaction with basement-derived fluid or organic matter is unlikely.

Noble gases (Ar, Kr, Xe) and halogens (Cl, Br, I) in fluid inclusions from the Athabasca Basin (Canada): Implications for unconformity-related U deposits

Antonin Richard [a,*], Mark A. Kendrick [b], Michel Cathelineau [a]

[a] GeoRessources UMR 7359, Université de Lorraine, CNRS, CREGU, Vandoeuvre-lès-Nancy, France

[b] Research School of Earth Sciences, Australian National University, Canberra, ACT 0200, Australia

* Corresponding author: Antonin Richard, GeoRessources UMR 7359, Université de Lorraine, Faculté des Sciences et Technologies, Entrée 3B - bureau A609, Boulevard des Aiguillettes BP 70239, 54506 Vandoeuvre-lès-Nancy Cedex, France

Phone : +33 3 83 68 47 37

Fax : +33 3 83 68 47 01

Mail : antonin.richard@univ-lorraine.fr

Abstract

The formation of unconformity-related uranium deposits in the Proterozoic Athabasca Basin (Canada) involved basin-scale circulation of U-bearing brines during high-grade diagenesis (150-200°C) at ~1.6-1.5 Ga. The UO_2 ores occur both sides of the unconformity and are associated with extensive brecciation and illite-sudoite-dravite alteration. Quartz and dolomite cementing veins and breccias are associated with alteration and mineralisation and contain a fairly uniform population of fluid inclusions characterised by variable Na:Ca and salinities of 25-35 wt.% salts and high U concentrations of up to 600 ppm U. In order to further constrain the origin of these U-rich brines, we analysed the naturally occurring isotopes of Ar, Kr and Xe, together with halogens (Cl, Br and I), K, Ca and U in irradiated quartz and dolomite samples containing representative fluid inclusions. This was achieved by the noble gas method for halogen measurement (extended ^{40}Ar-^{39}Ar methodology) using a combination of noble gas extraction techniques.

The fluid inclusions opened by crushing quartz and dolomite samples in vacuum have similar molar Br/Cl ratios of 5.8×10^{-3} to 10.4×10^{-3}, and molar I/Cl ratios of 1.8×10^{-6} to 8.2×10^{-6}. These compositions lie over the top half of the modern-day seawater evaporation trajectory, consistent with the fluids deriving the bulk of their salinity by subaerial evaporation of seawater, beyond the point of halite saturation. The I/Cl ratios are much lower than is typical of fluids that have interacted with I-rich organic matter present in many sedimentary basins or fluid inclusions found in Mississippi Valley type (MVT) Pb-Zn ore deposits. This is significant because provided the U-rich fluid inclusions are representative of the ore-stage fluids, the low I/Cl ratios of the fluid inclusions do not favour fluid interaction with organic matter (or hydrocarbons), as a major process for localizing U mineralisation.

The majority of samples contain fluid inclusions with age-corrected $^{40}Ar/^{36}Ar$ of between the modern atmospheric value of ~300 and 450. These values are considered

representative of the fluid's initial composition and are typical of upper crustal sedimentary formation waters. The fluid inclusions non-radiogenic $^{84}Kr/^{36}Ar$ and $^{129}Xe/^{36}Ar$ ratios are slightly enriched in ^{129}Xe relative to air and the fluid inclusions are estimated to contain 0.5-17.3 × 10^{-10} mol g^{-1} ^{36}Ar which is up to twenty times the ^{36}Ar concentration of air-saturated seawater. The data are interpreted to reflect acquisition of atmospheric noble gases from sedimentary rocks and suggest acquisition of radiogenic ^{40}Ar within K-rich basement rocks, that would have been an important source of excess ^{40}Ar, was limited by temperatures of less than 200ºC.

Taken together the halogen and noble gas composition of the U-bearing fluid inclusions are strongly controlled by subaerial evaporation and subsequent interaction with sedimentary rocks, showing that low temperature evaporitic brines dominated the mineralising system. Mineralisation is unlikely to have been triggered by fluid interaction with organic matter, or mixing with voluminous basement-derived fluids; however, the data do not completely preclude a role for volumetrically minor fluid or gas phases introduced by deep-seated basement faults preferentially located at the sites of mineralisation.

Keywords

Unconformity-related uranium deposits

Fluid inclusions

Halogens

Noble gases

Athabasca

1. Introduction

Spectacularly high grade and large tonnage deposition of uraninite (up to 200 kt of U at 20% U on average at McArthur River) has occurred in sedimentary rocks close to the basement unconformity of the Paleoproterozoic Athabasca Basin (Saskatchewan, Canada) (Jefferson et al., 2007; Kyser and Cuney, 2008). These occurrences attest to protracted basin-scale circulation of U-bearing fluids through sedimentary and basement rocks concurrent with sediment diagenesis at temperatures of 150-200°C (e.g. Hoeve and Sibbald, 1978; Kotzer and Kyser, 1995; Derome et al., 2005; Boiron et al., 2010; Richard et al., 2012).

This style of "unconformity-related" uranium mineralisation is unique to a restricted number of Proterozoic basins including the Athabasca and Thelon basins of Canada (e.g. Renac et al., 2002; Beyer et al., 2011) and the Kombolgie Basin of Northern Australia (Derome et al., 2003a, 2007; Polito et al., 2011). However, comparable processes may have been responsible for the famous Oklo U deposits in the Franceville Basin (Gabon), which on account of their high grades and slightly greater age formed natural nuclear reactors at ~2 Ga (e.g. Shukolyukov et al., 1976; Mathieu et al., 2000; Meshik et al., 2004; Boiron et al., 2010). The occurrence of these deposits may be restricted because their genesis is facilitated by the presence of a U-rich basement (10-100 ppm U), such as underlies many Paleoproterozoic terranes (Cuney, 2010). Furthermore, high porosity, kilometre-thick quartz sandstones, that are common in the basal section of the mineralised basins, acted as essential reservoirs for voluminous saline fluids, that enabled efficient fluid convection, suitable for transport of oxidised U(VI) from basement and/or sedimentary sources to the sites of deposition (Kyser et al., 2000).

The UO_2 ores in the Athabasca Basin are closely associated with intense illite-sudoite-dravite alteration in both basin and basement rocks and multiple generations of quartz and dolomite that form sandstone silicifications as well as veins and breccia cements (e.g. Hoeve

and Sibbald, 1978; Pagel et al., 1980; Kotzer and Kyser, 1995; Derome et al., 2005). Similar high salinity brine inclusions have been found in sandstone silicifications, quartz and dolomite vein and breccia cements as well as secondary fluid inclusions planes in basement magmatic and metamorphic quartz from both mineralised and barren altered areas and have been implicated as the dominant fluid involved at the time of alteration and mineralisation by several workers (e.g. Pagel et al., 1980; Kotzer and Kyser, 1995; Derome et al., 2005; Mercadier et al., 2010; Richard et al., 2010, 2012).

The origin of the brines and the fluid/rock interactions they underwent have been assessed by a variety of techniques applied to fluid inclusions and their host minerals (quartz and dolomite) in a number of deposits including those studied here. Microthermometry, LA-ICP-MS and synchrotron-SRF and XANES analyses show that the brines have temperatures of 150-200°C, salinities of 25-35 wt.% salts, variable Na:Ca ratios with NaCl-rich (Na>Ca>Mg>K) and $CaCl_2$-rich (Ca>Mg>Na>K) end-members, and that the fluid inclusions contain up to 600 ppm U(VI) (e.g. Pagel et al., 1980; Kotzer and Kyser, 1995; Derome et al., 2005; Richard et al., 2010, 2012, 2013a). Quartz and dolomite vein and breccia cements have been investigated isotopically for their O isotopic composition and these data show that quartz- and dolomite-forming fluids (trapped as fluid inclusions) are isotopically similar to the fluids responsible for deposit scale illite-sudoite-dravite alteration (Richard et al., 2013b). Furthermore, the fluid inclusions halogen (Cl, Br) composition (obtained by crush-leach ion chromatography and LA-ICP-MS analysis of individual fluid inclusions); the Cl isotope composition of fluid inclusion leachates; and the B isotope composition of dravite have been investigated. These studies favour subaerial evaporation of seawater as the dominant mechanism for generating the fluids high salinities (Richard et al., 2011; Leisen et al., 2012; Mercadier et al., 2012).

Despite these powerful constraints on the nature of the ore fluids, there remain several open questions, that will be addressed by the current study which extends the analysis of halogens in the fluid inclusions, to include I, and combines the measurements of halogens with noble gases. Firstly, it is debatable if NaCl-rich and $CaCl_2$-rich brines represent distinct fluids, derived for example by evaporation of seawater to different degrees, or if the Ca-Na-Mg-K variation simply reflects variable fluid-rock interactions. Secondly, the basement rocks represent a potential U source (Hecht and Cuney, 2000; Mercadier et al., 2013), but the extent to which basinal fluids were convected into the basement and equilibrated with basement rocks is poorly constrained. Thirdly, the mechanism for the reduction of U(VI) to U(IV) and subsequent precipitation of UO_2 is still contentious. Fluid-rock interaction, fluid-organic matter interaction and mixing with deeply-sourced fluids are alternatively invoked (e.g. Hoeve and Sibbald, 1978; Wilson and Kyser, 1987; Alexandre and Kyser, 2006).

The noble gases can provide new insights on fluid interaction with basement rocks, or the presence of deeply-sourced fluid components because old K-rich basement rocks, such as the 1.8 Ga to Archean age rocks underlying the Athabasca Basin (Card et al., 2007) would be expected to have high $^{40}Ar/^{36}Ar$ ratios (e.g. Kendrick et al., 2011a,b). In contrast, the relatively K-poor overlying sediments (deposited from 1.76 Ga; Ramaekers et al., 2007) that contained air saturated waters and trapped atmospheric noble gas components (e.g. Podosek et al., 1980) are more likely to preserve low $^{40}Ar/^{36}Ar$ values. Iodine is an essential element for life and its incorporation into organic matter means that fluid I/Cl ratios are a sensitive indicator for fluid interaction with organic matter (Kendrick et al., 2011c). The measurement of noble gases (Ar, Xe, Kr) and halogens (Cl, Br, I) by extended $^{40}Ar/^{39}Ar$ methodology provides simultaneous analysis of K, Ca and U (Kendrick, 2012), meaning noble gas and halogen signatures can be closely related to the fluids U and cation content (indicative of fluid-rock interaction). Finally, determination of Cl and Br, with I, by this methodology,

provides an independent confirmation of ion chromatographic and LA-ICP-MS Br and Cl analyses (Richard et al., 2011; Leisen et al., 2012) and additional plots that include I for assessing the extent to which the data 'fit' the suggested fluid origin by seawater evaporation.

2. Geological setting, sampling and fluid inclusions

2.1. The Archean to Paleoproterozoic Basement

The Athabasca Basin overlies basement rocks of the Archean to Paleoproterozoic Western Churchill Province which is further divided into the Rae Subprovince in the west and the Hearne Subprovince in the east by the Northeast-trending Snowbird tectonic zone (Hoffman, 1990; Card et al., 2007) (Fig. 1). The basement lithologies comprise Archean gneisses, Paleoproterozoic metapelites and mafic to felsic intrusions, that were all strongly metamorphosed during the ~2.0-1.9 Ga Thelon-Talston orogeny in the west, and the ~1.9-1.8 Ga Trans-Hudson orogeny in the east (Chiarenzelli et al., 1998; Annesley et al., 2005; Card et al., 2007). Most of the unconformity-related uranium deposits in the Athabasca Basin are located in the vicinity of the Wollaston-Mudjatik transition zone (WMTZ) that separates the Wollaston and Mudjatik lithostructural domains of the Hearne Subprovince (Annesley et al., 2005; Fig. 1).

2.2. The Paleoproterozoic Athabasca Basin

The sedimentary rocks of the Athabasca Basin, known as the Athabasca Group, unconformably overly the crystalline basement, and sediment deposition started at ~1.75 Ga (Ramaekers et al., 2007; Fig. 1). The current maximum thickness of the sedimentary cover is ~1.5 km (Rumple Lake), but it is thought to have reached a maximum thickness of ~5 km, based on P-T estimations from fluid inclusion studies (Pagel, 1975; Derome et al., 2005). The oldest sediments in the Athabasca Group comprise a ~1 km thick basal sequence of fluvial to

marginal marine quartz-rich sandstones known as the Fair Point, Read, Smart and Manitou Falls Formations. The overlying Lazenby Lake and Wolverine Point Formations comprise marine sandstones, phosphatic siltstones and phosphatic mudstones. These are overlain by fluviatile sandstones of the Locker Lake and Otherside Formations, shales of the Douglas Formation and finally stromatolitic carbonates of the Carswell Formation (Ramaekers et al., 2007).

2.3. The Mesoproterozoic unconformity-related uranium deposits in the Athabasca Basin

The peculiarity of unconformity-related uranium deposits in the Athabasca Basin is that they can reach extremely high grade and tonnage. For example, the giant McArthur River deposit in the Athabasca Basin, which is included in the current study, has produced ~200,000 tonnes of U ore at a grade of 20 wt.% U (Jefferson et al., 2007).

The Athabasca unconformity-related U ores are typically located within ~100-400 m of the unconformity between the Archean to Paleoproterozoic basement and the Paleoproterozoic sedimentary cover, close to graphite-rich basement faults that occur preferentially within metapelite units. Of the deposits included in this study, the P-Patch and Eagle Point deposits are entirely hosted by crystalline basement (Mercadier et al., 2010; Cloutier et al., 2011). The McArthur River deposit occurs on both sides of the unconformity (e.g. Derome et al., 2005). The Rabbit Lake is located at the very margin of the preserved sedimentary cover and is presently entirely hosted in the basement but may have been spatially connected to the unconformity prior to erosion (e.g. Hoeve and Sibbald, 1978; Heine, 1986; Alexandre et al., 2005).

The main alteration features associated with UO_2-ores include: (i) partial to complete replacement of the initial basement minerals (K-feldspar, biotite, plagioclase, hornblende) by an illite + sudoite (Mg-chlorite) ± dravite (Mg-tourmaline) assemblage (e.g. Alexandre et al.,

2005; Mercadier et al., 2010), as well as the precipitation of quartz, illite, sudoite and dravite in the sandstones (e.g. Kotzer and Kyser 1995; Lorilleux et al., 2002; Kister et al., 2006); (ii) quartz dissolution in basement rocks as well as in the sandstones with hydraulic and chemical brecciation (e.g. Lorilleux et al., 2003; Mercadier et al., 2010); (iii) precipitation of UO_2 in the alteration-related porosity as well as in veins and breccias also cemented by dravite ± quartz ± dolomite ± bitumen (e.g. Hoeve and Sibbald, 1978; Derome et al., 2005) and (v) rare earth element mobilization and redistribution among aluminium phosphate-sulphate minerals such as florencite, goyazite and svanbergite and UO_2 (e.g. Fayek and Kyser, 1997; Gaboreau et al., 2007; Mercadier et al., 2011a). A simplified mineral paragenetic sequence summarizing petrographical observations of U deposits throughout the Athabasca Basin is shown in Fig. 1.

A wide range of ages spanning 1.6-0.9 Ga have been reported for U-related mineralisation and alteration minerals in the Athabasca Basin (e.g. Cummings and Krstic, 1992; Fayek et al., 2002; Alexandre et al., 2009). However, the most recent geochronological data show that pre-ore illite and sudoite preserve maximum $^{40}Ar/^{39}Ar$ ages of ~1670 Ma and syn-ore illite preserves a maximum $^{40}Ar/^{39}Ar$ age of ~1580 Ma that is similar to the maximum U-Pb ages of 1540 ± 20 Ma obtained for uraninite (Alexandre et al., 2009). These data can be interpreted to indicate alteration and mineralisation spanned a period of <150 Ma between 1670 and 1500 Ma, and the younger ages recorded by both the $^{40}Ar/^{39}Ar$ and U/Pb systems result from remobilisation of UO_2 and partial ^{40}Ar or Pb loss, which has probably occurred multiple times up until the present day (e.g. Alexandre et al., 2009; Fayek et al., 2002; Mercadier et al., 2011b).

2.4. Quartz and dolomite cements and their fluid inclusions in the ore-forming process

Many workers agree quartz cements are closely spatially associated with the main alteration minerals (illite, sudoite, dravite) and UO_2 (e.g. Dahlkamp, 1978; Hoeve and

Sibbald, 1978; Wilson and Kyser, 1987; Kotzer and Kyser, 1995; Fayek and Kyser, 1997; Kyser et al., 2000; Lorilleux et al., 2002; Derome et al., 2005; Kyser and Cuney, 2008; Ng et al., 2013). Furthermore, carbonates (including dolomite) have been consistently described as gangue minerals in the Rabbit Lake, Shea Creek and McArthur River deposits (Hoeve and Sibbald, 1978; Pagel et al., 1980; Hoeve et al., 1986; Heine, 1986; Lorilleux et al., 2002; Derome et al., 2005). As a consequence of this close association, fluid inclusions in the quartz and dolomite cements have been targeted as representative of the dominant fluid involved at the time of alteration and mineralisation. The following observations indicate that NaCl-rich and $CaCl_2$-rich brines were the dominant fluid involved from the pre-ore stage to the syn-ore stage and the post-ore stage: (i) sandstone silicifications, which are unanimously recognized as preceding the main UO_2 stage show primary NaCl-rich and $CaCl_2$-rich brine inclusions at Cluff Lake and McArthur River deposits (Pagel, 1975; Kotzer and Kyser, 1995; Derome et al., 2005); (ii) the increasing intensity of illite-sudoite-dravite alteration is related to the increasing abundance of secondary NaCl-rich and $CaCl_2$-rich brine inclusion planes in the magmatic and metamorphic quartz from basement rocks at the P-Patch deposit (Mercadier et al., 2011); (iii) quartz and dolomite cements in barren and mineralized veins and breccias are all filled by primary and pseudosecondary NaCl-rich and $CaCl_2$-rich brine inclusions in all the deposits studied here (Pagel et al., 1980; Kotzer and Kyser, 1995; Derome et al., 2005; Richard et al., 2011); (iv) LA-ICP-MS and synchrotron-SRF and XANES analyses have been applied to those NaCl-rich and $CaCl_2$-rich brine inclusions in both barren and mineralised samples and showed that they contain up to 600 ppm U(VI) (Richard et al., 2010, 2012, 2013a); (v) the O isotopic composition and these quartz and dolomite cements shows that cement-forming fluids (i.e. NaCl-rich and $CaCl_2$-rich brines) are isotopically equilibrated with illite, sudoite and dravite (Richard et al., 2013b) and (v) the B isotopic composition of dravite as well as Cl/Br ratios coupled with Cl isotope compositions of NaCl-rich and $CaCl_2$-rich

brine inclusions in quartz and dolomite cements indicate a common evaporated seawater origin for the dravite-forming fluids and the NaCl-rich and $CaCl_2$-rich brines (Richard et al., 2011; Leisen et al., 2012; Mercadier et al., 2012).

Some other workers have concluded from crosscutting relationships that quartz and dolomite cements postdate the main UO_2 stage meaning their fluid inclusions cannot be used to identify the ore fluids (e.g. Alexandre et al., 2005; Cloutier et al. 2009). Indeed, the relative timing of the alteration minerals, quartz and dolomite cements and the UO_2 can be ambiguous because mineral deposition is often cyclic (Dahlkamp, 1978; Hoeve and Sibbald, 1978) and the different stages are variably expressed in basement and sandstone lithologies (e.g. Kyser and Cuney, 2008; Alexandre et al., 2009). In addition, recurrent episodes of quartz dissolution have been identified (e.g. Derome et al., 2005) meaning the fluid inclusions in quartz and dolomite may not have recorded the entire fluid story. As a consequence, it is always debatable whether a given quartz or dolomite sample contains fluid inclusions which are fully representative of the fluids involved at the main UO_2 stage. However, as mentioned above, all fluid inclusion studies point to NaCl-rich and $CaCl_2$-rich brines as the dominant fluid involved.

2.5. Sampling for the current study

Seven samples from McArthur River (MAC54Qz), P-Patch (P48-2, P48-5), Rabbit Lake (RBL2 and RBL7) and Eagle Point (ES287-8, H3042-1), which are 4 of the best characterised deposits in the Athabasca Basin, were selected for the current study (Fig. 1; Fig. 2; Table 1). These samples show typical quartz and dolomite cements in veins and breccias and typical NaCl-rich and $CaCl_2$-rich brine inclusions as described in details elsewhere within alteration haloes as well as in barren and mineralized samples (e.g. Pagel et al., 1980; Kotzer and Kyser, 1995; Derome et al., 2005; Richard et al., 2010, 2011; Mercadier et al., 2011).

The samples were selected from varying depths into the basement lithologies, to a maximum of 263 m below the unconformity (H3042-1). The samples show variable degree of alteration, from relatively unaltered (H3042-1) to highly altered "bleached" (illite-sudoite-dravite alteration) (ES-287-8, P-48-5). This was undertaken to evaluate if a basement noble gas signature could be detected. Some samples contain quartz cement without dolomite (ES287-8, H3042-1, P48-2, P48-5, MAC54Qz) while others show quartz and dolomite cements, dolomite postdating quartz (RBL2 and RBL7). Quartz and dolomite cements in both veins (ES287-8, H3042-1, P48-2, P48-5) and breccias (MAC54Qz, RBL2 and RBL7) were selected. Together with quartz, veins and breccias are cemented by dravite or dravite+sulphides in samples H3042-1 and MAC54Qz respectively. Textural evidence suggests that dravite predates quartz which in turn predates sulphides. Despite the close association of the selected samples with mineralisation, none of the selected samples contain UO_2 ore within the hand-specimen sized section available from drill core. Barren samples were specifically selected to avoid possible artefacts related to post-entrapment production of nucleogenic noble gases modifying the fluid inclusions ^{36}Ar concentration (See Section 3).

The fluid inclusion characteristics of the selected samples have been described in Richard et al. (2011) and are summarised below. The selected quartz and dolomite samples are dominated by primary and pseudosecondary fluid inclusions of 5 to 25 µm in size in which a vapour phase occupies ~10% of the inclusion volume. The majority of inclusions have two phases (liquid + vapour) but up to ~25% contain three phases (liquid + vapor + halite) (Fig. 2; Table 1). A few of the inclusions contain haematite and/or phyllosilicate minerals (illite and chlorite as identified by Raman spectrometry by Derome et al., 2005) that are also interpreted as daughter minerals due to their constant volume within the fluid inclusions. This is significant because, it demonstrates that some of the fluid inclusions within the selected samples are saturated with respect to alteration minerals. The fluid inclusions

have a restricted range of salinity of ~25-35 wt.% salts, and homogenise into the liquid phase generally between 90 and 170°C. The relative abundances of different fluid inclusion types representative of NaCl and $CaCl_2$ brines, together with average salinities of fluid inclusions in each sample, are summarised in Table 1. In addition to the primary fluid inclusions that are of interest for investigating U mineralisation, the samples contain a low abundance of low-salinity secondary fluid inclusions similar to those described by Derome et al., (2005). The low abundance (<1%) and low salinity (1-10 wt.% eq. NaCl) of these secondary fluid inclusions implies they will make a negligible contribution to the Cl, Br, I, K, Ca and U compositions measured by bulk analysis of the fluid inclusion bearing samples in this study. However, each sample was analysed sequentially, by multiple *in vacuo* crushing analyses to test for sample heterogeneity and help asses if the secondary fluid inclusions significantly influenced the noble gas signatures (see Section 3).

3. Methodology

The halogens (Cl, Br, I), Ca, K and U were measured simultaneously with the naturally occurring noble gas isotopes of Ar, Kr and Xe using the noble gas method which is described in detail by Kendrick (2012) (see also Böhlke and Irwin (1992a) and Johnson et al. (2000)). Fluid inclusion bearing quartz and dolomite samples of 30-110 mg were irradiated for 50 hours in position 5c of the McMaster Nuclear Reactor, Canada (irradiation designated UM#37 on the 5th January 2010), to produce noble gas proxy isotopes ($^{38}Ar_{Cl}$, $^{80}Kr_{Br}$, $^{128}Xe_{I}$, $^{37}Ar_{Ca}$ $^{39}Ar_{K}$ and $^{134}Xe_{U}$) that are measured by noble gas mass spectrometry (Kendrick, 2012).

The irradiated samples were loaded into modified Nupro® valves, baked under ultra-high vacuum at ~100 ºC for 24-48 hrs to remove loosely adsorbed noble gases, and then analysed by in vacuum crushing. Short crushing experiments in Nupro® valves release naturally occurring and neutron-produced noble gas isotopes from fluid inclusions and

contributions from the mineral matrix are negligible (Kendrick and Phillips, 2009). Each sample was analysed by multiple crushes, enabling compositional variations resulting from fluid inclusion heterogeneity to be assessed (Section 2.5). The crushed residues of 6 quartz samples were then loaded into Sn-foil packets and fused in a 20 minute heating step at 1600°C using a tantalum resistance furnace. Fusion removes noble gases from remaining fluid inclusions and the mineral matrix, meaning the combined *in vacuo* crushing and fusion analyses provide complementary information.

The noble gas isotopes released by *in vacuo* crushing and fusion were purified by standard gettering procedures over a period of 20 minutes and measured in peak jumping mode on the MAP-215 noble gas mass spectrometer at the University of Melbourne. The isotopes of Ar where measured on a Faraday detector whereas the less abundant isotopes of Kr and Xe were measured on the more sensitive electron multiplier detector (Kendrick, 2012).

Ratios of Cl to Br, I, Ca, K and U are obtained from the measured noble gas proxy isotopes and monitored production ratios. Production ratios for $^{38}Ar_{Cl}/Cl$, $^{37}Ar_{Ca}/Ca$ and $^{39}Ar_{K}/K$ were monitored using the Hb3Gr and GA1550 ^{40}Ar-^{39}Ar flux monitors, whereas the $^{128}Xe_{I}/I$ and $^{80}Kr_{Br}/Br$ production ratios were monitored using four scapolite standards (Kendrick, 2012; Kendrick et al., 2013). Standard corrections were made for Ar interference reactions based on K-glass and CaF_2 monitors and U-derived ^{84}Kr (Kendrick, 2012). Unfortunately, fusion analyses were undertaken more than a year after sample irradiation, meaning ^{37}Ar, which has a half life of 35 days could not be measured. Fluid inclusion ^{36}Ar, ^{40}Ar and U concentrations have been calculated from the measured ratios (X/Cl) and the fluid inclusion salinity determined via microthermometry and given in Table 1.

The noble gas method provides very low detection limits, and machine blanks for crushing samples in modified Nupro® valves that typically account for <1% of sample gas. The Br/Cl and I/Cl ratios are reported relative to scapolite standards that have

reproducibilities of ~3% for Br/Cl and ~5 % for I/Cl (1σ; see Kendrick 2012; Kendrick et al., 2013). The precision of the K/Cl, Ca/Cl and U/Cl measurements were more variable and were limited by the low abundance of the noble gas proxy isotopes ($^{39}Ar_K$, $^{37}Ar_{Ca}$ and $^{134}Xe_U$) available for analysis in several cases. The U measurements are based on a $^{134}Xe_U$/U production ratio calculated from the monitored neutron fluence and U cross section, rather than a U monitor (Kendrick 2012). This means that while real differences in the U concentration can be precisely monitored, the absolute U values could be systematically out by up to ~20% in all the samples. The accuracy of the fluid inclusion concentrations of U, ^{40}Ar and ^{36}Ar is further limited to the ~30% level by the variability of fluid inclusion salinities within each sample (~25-35 wt.% salts; see Section 2.5).

Finally, post entrapment modification of fluid inclusion Ar-isotope signatures are considered to be a minor artefact in this study. Firstly, the low K content of the samples means that despite the samples great age (Section 2.3), post-entrapment production of radiogenic $^{40}Ar_R$ is negligible, necessitating a correction of less than 5% for the majority of samples (Table 2). Secondly, we present data for samples situated >1 m from U ore, which minimises the possible influence of post-entrapment nucleogenic reactions modifying fluid inclusion ^{36}Ar concentrations, because neutrons have an attenuation distance of ~1 m in silicate rocks (Ballentine and Burnard, 2002; Hu et al., 2009).

4. Results

The halogen and noble gas results obtained by *in vacuo* crushing of quartz and dolomite hosted fluid inclusions are summarised in Table 2, and the results obtained by fusing selected crushed quartz samples are summarised in Table 3.

Quartz and dolomite hosted fluid inclusions extracted by *in vacuo* crushing have molar Br/Cl values between $(5.8 \pm 0.1) \times 10^{-3}$ and $(10.4 \pm 0.1) \times 10^{-3}$, I/Cl values between (1.8 ±

0.1) × 10^{-6} and (8.2 ± 0.2) × 10^{-6} (Fig. 3), and K/Cl values between 0.017 ± 0.005 and 0.056 ± 0.002 that are typical of crustal fluids (Fig. 4; Fig. 5; Fig. 6). Quartz-hosted fluid inclusions extracted by *in vacuo* crushing have Ca/Cl values of between 0.06 ± 0.04 and 0.19 ± 0.06 (Fig. 4; Fig. 5; Fig. 6), but Ca data are not reported for dolomite samples for which there was a significant matrix contribution. The *in vacuo* crushing data show fluid inclusion U/Cl values vary from 2.5 × 10^{-6} to 1.4 × 10^{-4} in the majority of samples (Fig. 5). Based on the mean fluid inclusion salinities given in Table 1, the fluid inclusions are therefore indicated to contain between 3 and 170 ppm U.

The *in vacuo* crushing analyses yield imprecise ^{40}Ar-^{39}Ar ages of up to 4 Ga, that are much older than the age range reported for U-related alteration minerals (Cummings and Krstic, 1992; Fayek et al., 2002; Alexandre et al., 2009), demonstrating that excess ^{40}Ar is trapped in the fluid inclusions [excess ^{40}Ar ($^{40}Ar_E$) is defined as parentless non-atmospheric ^{40}Ar that was not generated by decay of ^{40}K within the sample]. The ^{40}Ar/^{36}Ar ratios obtained by *in vacuo* crushing range from 302 to 480 and are higher than the modern atmospheric value of 296 and considered fairly representative of the fluid inclusions initial composition at the time of trapping (Table 2). The maximum correction possible for post-entrapment production of ^{40}Ar within the fluid inclusions is only ~5%, based on the measured K abundances of the fluid inclusions and an assumed age of 1.6 Ga (Table 2).

In vacuo crushing yields fluid inclusion Cl/^{36}Ar values of between (2.7 ± 0.1) × 10^6 and (86 ± 1) × 10^6 and repeat crushing analyses of the dolomite and quartz samples show ^{40}Ar/^{36}Ar and Cl/^{36}Ar are correlated in several of the samples (Fig. 6). The majority of the Ar mixing lines converge on an end-member with low Cl/^{36}Ar and ^{40}Ar/^{36}Ar of close to the modern atmospheric value of 296, and the slopes of Ar mixing lines forced through the atmospheric ^{40}Ar/^{36}Ar ratio represent the samples average $^{40}Ar_E$/Cl ratio (Fig. 6).

The highest $^{40}Ar/^{36}Ar$ values and $Cl/^{36}Ar$ values obtained by *in vacuo* crushing each sample is suggested as most representative of the NaCl and $CaCl_2$ fluid inclusions (Fig. 6). The sample specific $Cl/^{36}Ar$ versus $^{40}Ar/^{36}Ar$ mixing lines (Fig. 6), probably result from mixing the dominant NaCl and $CaCl_2$ brine inclusions with low salinity secondary fluid inclusions present in the samples (see Section 2.5); however, the mixing lines could also result if a modern air contaminant was trapped in voids within the samples. Based on combining the fluid inclusions $^{40}Ar_E/Cl$ ratios of between 0.04×10^{-6} and $(2.7 \pm 0.3) \times 10^{-6}$ (Table 2) with the mean salinity of brine inclusions in each sample, we calculate the fluid inclusions contain 0.02×10^{-8} to 1.4×10^{-8} mol g^{-1} of $^{40}Ar_E$. Based on the maximum $Cl/^{36}Ar$ value obtained for each sample (considered representative of the NaCl and $CaCl_2$ brine inclusions) and the mean fluid inclusion salinity, we obtain fluid inclusion ^{36}Ar concentrations of 0.5×10^{-10} to 17.3×10^{-10} mol g^{-1} (Table 2).

The fluid inclusion $^{129}Xe/^{36}Ar$ and $^{84}Kr/^{36}Ar$ values obtained by *in vacuo* crushing are reported as fractionation values relative to air (Fig. 6). The fractionation values are defined as $F(X/^{36}Ar)_{air} = (X/^{36}Ar)_{sample}/(X/^{36}Ar)_{air}$, where X = ^{84}Kr or ^{130}Xe, and air has $F(^{129}Xe/^{36}Ar)_{air}$ and $F(^{84}Kr/^{36}Ar)_{air}$ values of one. The fluid inclusion $F(^{84}Kr/^{36}Ar)_{air}$ ratios are close to 1 but $F(^{129}Xe/^{36}Ar)_{air}$ varies from ~1 to 2.7 ± 0.2 demonstrating a significant enrichment in ^{129}Xe relative to air (Table 2).

Fusing previously crushed samples at 1600°C released slightly less $^{38}Ar_{Cl}$ than *in vacuo* crushing and similar proportions of ^{36}Ar as *in vacuo* crushing (Table 2; Table 3). The fusion data are characterised by Br/Cl ratios that are typically 30-40 % lower than the *in vacuo* crushing values and K/Cl and U/Cl values that are more variable than the *in vacuo* crushing values (Table 2; Table 3). The maximum K/Cl ratio of 6.5 obtained by fusion (Table 3) is higher than can be explained by decrepitation of fluid inclusions which have Na- or Ca-rich compositions (Richard et al., 2010) and are indicated to have K/Cl of <0.1 by the *in*

vacuo crushing data (note that pure sylvite has K/Cl of 1). Furthermore, fusion yields imprecise ^{40}Ar-^{39}Ar ages of 0.8-1.4 Ga that overlap the range of ages of 1.2-1.6 that have previously been reported for K-bearing alteration minerals (Alexandre et al., 2009), showing mineral impurities make a significant contribution to the irradiation produced noble gases released by fusion (Table 3). Finally, $F(^{84}Kr/^{36}Ar)_{air}$ and $F(^{129}Xe/^{36}Ar)_{air}$ ratios obtained by fusion are uniformly greater than air with the maximum $F(^{129}Xe/^{36}Ar)_{air}$ of 52 demonstrating a very significant enrichment of atmospheric Xe relative to Ar (Table 3).

5. Discussion

5.1. Comparison of in vacuo crushing and fusion data

5.1.1 Fluid inclusion ^{40}Ar/^{36}Ar ratios and ^{40}Ar-^{39}Ar ages

The simplest interpretation of the argon data is that the age-corrected ^{40}Ar/^{36}Ar ratios of <450 and the K/Cl ratios of 0.02-0.06 obtained by *in vacuo* crushing are representative of the fluid inclusions at the time of trapping (Table 2). In contrast, fusing previously crushed samples gave a maximum K/Cl of 6.5, and U/Cl ratios of 200-300 times higher than *in vacuo* crushing, suggesting ^{39}Ar and ^{134}Xe were released from K and U mineral impurities in the crushed samples by heating (e.g. Kendrick et al., 2001; 2006). The similarity of apparent ages of 0.8-1.4 Ga obtained by fusion of the quartz samples and other K-bearing minerals (Alexandre et al., 2009) is consistent with the ages having been obtained from mineral impurities within the quartz rather than the fluid inclusions. Given the mineral impurities must be very small to have avoided detection during careful sample preparation under a binocular microscope, and small mineral impurities have very low retentivities to ^{40}Ar, the apparent ages are likely to represent cooling ages and are not related to the timing of mineralisation (see Kendrick et al., 2006).

One possible complexity in the above interpretation is that the $^{40}Ar/^{36}Ar$ measured by *in vacuo* crushing might be significantly higher than the fluid inclusions initial value if significant ^{40}Ar was lost from phyllosilicate daughter minerals into the host fluid inclusion. However, as crustal $^{40}Ar/^{36}Ar$ ratios vary from ~300 up to at least 50,000 (Kendrick et al., 2011b) this does not affect interpretation of the current data that have measured $^{40}Ar/^{36}Ar$ ratios of <480 and preferred values of <460 after a correction for 1.6 Ga of post entrapment in growth (Table 2).

5.1.2. Halogen ratios

The Br/Cl values obtained by *in vacuo* crushing are 30-40 % higher than the values obtained by fusion (Table 2; Table 3). It is difficult to establish the cause of this discrepancy with certainty; however, our favoured explanation is that *in vacuo* crushing releases noble gases from fluid inclusions and fusion releases noble gases from fluid inclusions in the crushed sample and mineral impurities in the quartz matrix, phyllosilicates or mica, which must explain K/Cl ratios of >1 measured by fusion (Table 3), and could also contribute significant Cl (200-500 ppm Cl in illite and sudoite the after Richard et al., 2011), with very little Br (e.g. Kendrick, 2012), that could potentially reduce the Br/Cl ratio measured by fusion.

An alternative explanation that high Br/Cl ratios could result from retention of $^{38}Ar_{Cl}$ in halite daughter minerals during *in vacuo* crushing (Kendrick et al., 2001) is possible, but:(i) samples containing fluid inclusions with daughter minerals sometimes give the same Br/Cl ratios by both techniques (Fisher and Kendrick, 2008), and *in vacuo* crushing sometimes gives higher Br/Cl than stepped heating samples hosting fluid inclusions without daughter minerals (Kendrick, unpublished data), suggesting daughter crystals are minor $^{38}ArCl$ reservoirs; (ii) daughter mineral-bearing inclusions are minor in some of the current samples and were not

observed in samples ES287-10, RBL2Qz or RBL2Carb (Table 1; Section 2.5); and (iii) whereas Br/Cl measured by stepped heating is systematically lower than the *in vacuo* crushing data, the I/Cl ratio obtained by fusing ES287-10 and H304-2 is higher than obtained by *in vacuo* crushing (Table 2; Table 3). This difference cannot be explained by the retention of ^{38}ArCl in halite daughter minerals, but could potentially be explained by the presence of organic contaminants and mineral impurities in the quartz matrix.

A final possibility is that fluid inclusions with different sizes, or different occurrences (e.g. isolated versus annealed fractures), have different Br/Cl and I/Cl ratios, and that *in vacuo* crushing and fusion release noble gases from these fluid inclusions differently. While we cannot yet preclude this possibility, if it were true we would expect non-systematic variation in Br/Cl between the two techniques, whereas to date, every time there has been a discrepancy the lower Br/Cl ratios is obtained by stepped heating (this study; Kendrick et al., 2001; 2007).

In summary, we believe the *in vacuo* crushing data emphasised throughout the remainder of this discussion are fairly representative of the fluid inclusions in our samples, and that Cl-bearing mineral impurities in the quartz matrix probably contribute to the fusion results. For simplicity we focus on the *in vacuo* crushing results; however, it should be noted that this does not greatly change the interpretations below and sample average Br/Cl and I/Cl, obtained by combining the *in vacuo* crushing and fusion data in Table 2 and Table 3, would be within ~20 % of the *in vacuo* crushing analyses.

5.2. Origin of fluid inclusion salinity

The fluid inclusion molar Br/Cl versus I/Cl values determined for quartz- and dolomite-hosted brine inclusions by *in vacuo* crushing using the noble gas method are compared with modern seawater evaporation trends and the compositions of other important

fluid and mineral reservoirs in Fig. 3. The fluid inclusion data lie over the top part of the modern seawater evaporation trajectory (Zherebtsova and Volkova, 1966).

The new Br/Cl values obtained by *in vacuo* crushing (5.8×10^{-3} to 10.4×10^{-3}) are higher than those measured previously on the same samples by crush-leach ion chromatography (3×10^{-3} to 6×10^{-3}; Richard et al., 2011; Fig. 3), or determined for individual fluid inclusions in from McArthur River by LA-ICP-MS (1×10^{-3} to 5×10^{-3}; Leisen et al., 2012); however, crush-leach ion chromatography has given Br/Cl of up to 10×10^{-3} for Eagle Point dolomite and 8×10^{-3} for McArthur River dolomite (Richard et al., 2011). Therefore although the Br/Cl ratios obtained in this study are higher than those reported previously (Fig. 3), all of the techniques give overlapping results on large sample sets, and some of the difference for the common samples analysed by both techniques could be related to sample heterogeneity. Further work to inter-calibrate these different techniques for measuring Br and Cl (e.g. Hammerli et al., 2013; Kendrick et al., 2013); and detailed comparison of the methods used for extracting fluid inclusions is clearly desirable (e.g. crush-leach; *in vacuo* crushing; stepped heating). However, as all the techniques give Br/Cl of mostly greater than seawater, the differences do not strongly influence the interpretation of the data in the current study. We focus on the *in vacuo* crushing Br/Cl data obtained here because this technique has very high internal precision and provides simultaneous I/Cl analyses.

The *in vacuo* crushing Br/Cl and I/Cl ratios lie over the top part of the modern day seawater evaporation trajectory (Fig. 3). Taken together with the high chlorinity of the fluid inclusions (~5000 mmol/kg solution in Fig. 3; ~25-35 wt.% salts) this provides strong evidence that the fluids derived the bulk of their salinity by subaerial evaporation of seawater beyond the point of halite saturation (Fig. 3). However, despite the indicated importance of seawater evaporation, this mechanism produces residual brines with maximum salinities of

~30 wt.% salts (Zherebtsova and Volkova, 1966; Nissenbaum, 1977). The existence of halite saturated fluid inclusions with visible daughter crystals and total salinities of ~35 wt.% salts in these samples (Fig. 2), therefore requires a further mechanism to increase the fluids salinity above the point of halite saturation.

The most likely mechanism for increasing the brines salinity above ~30 wt.% salts was probably H_2O consumption during illitisation and chloritisation of feldspar during basement alteration. Fluid inclusions show progressively higher salinities in the areas of the basement that have been most intensely altered by illitisation and chloritisation (Mercadier et al., 2010). Another mechanism that could have increased the salinity of the evaporitic brine above 30 wt.% would have been the dissolution of evaporites that might have been present within overlying sediments. However, although dissolution of evaporites would increase the fluids salinity, it would also move the fluids Br/Cl and I/Cl composition back down the seawater evaporation trajectory (Fig. 3). As a result, evaporite dissolution would lead to the fluids with the highest salinities tending to have the lowest Br/Cl values, which is not observed (Fig. 3).

The measurement of I/Cl, in addition to Br/Cl, is important because sedimentary formation waters can evolve high I/Cl and Br/Cl values as a result of interaction with organic matter (Kendrick et al., 2011c). The low I/Cl values of the U-related fluids indicate very little interaction with organic-rich sediments or hydrocarbons and the elevated Br/Cl cannot be attributed to an organic Br component as previously suggested by Pagel and Jaffrezic (1977) and Pagel et al. (1980). The lack of organic I and Br components in the ore fluids related to unconformity U mineralisation is in stark contrast to the majority of formation waters and ore fluids related to sediment-hosted Zn-Pb mineralisation in Mississippi Valley-type ore deposits which have I/Cl of 10-1000 $\times$ 10^{-6} (Fig. 3; Kendrick et al., 2011c). The new results demonstrate the NaCl-rich and $CaCl_2$-rich brines do not contain a significant organic component.

In summary, the halogen data indicate seawater evaporation as the dominant source of salinity and that illitisation and chloritisation were probably important for further increasing fluids salinity. The dominant source of salinity is therefore similar to that suggested by the lower Br/Cl ratios obtained by ion chromatography methods previously (Richard et al., 2011). The main uncertainty resulting from the different Br/Cl ratios (Fig. 3) is the extent to which minor processes such as illitisation or evaporite dissolution have modified the bittern brines.

5.3. Origin of fluid inclusion cation (Ca, K, U) composition

The bulk fluid inclusion molar Ca/Cl and K/Cl values determined by *in vacuo* crushing of quartz and dolomite samples are shown in Fig. 4 together with the approximate fields of the most NaCl-rich and $CaCl_2$-rich fluid inclusion end-members analysed by LA-ICP-MS (Richard et al., 2010) and microthermometry (Derome et al., 2005).

Most of the *in vacuo* crushing analyses have Ca/Cl of less than 0.15 that suggest the samples are dominated by NaCl-rich fluid inclusions even though $CaCl_2$-rich inclusions have been observed in some of the samples (Table 1). The extreme NaCl-rich and $CaCl_2$-rich end-member compositions can only be defined by analysing individual fluid inclusions (e.g. Richard et al., 2010). However, the *in vacuo* crushing data do not lie on a simple mixing trend between the suggested end-members (Fig. 4), which is most easily explained if the K/Cl composition of NaCl-rich fluid inclusions is more variable than previously suggested (Fig. 4).

The fluid inclusion molar Ca/Cl and K/Cl values are plotted against Br/Cl, I/Cl and U/Cl values in Fig. 5. Evaporation trends of $MgSO_4$-rich seawater (similar to modern day seawater) and $CaCl_2$-rich seawater are shown in Fig. 5, because the actual composition of seawater at the time of U mineralisation is unknown and seawater is suggested to have oscillated between these types over Earth history (Lowenstein et al., 2001; Hardie 2003; Kovalevych et al., 2006). In contrast, to Br/Cl and I/Cl data shown in Fig. 3, the fluid

inclusions Ca/Cl and K/Cl values cannot be easily related to any particular stage of either seawater evaporation trajectory (Fig. 5). Both the K/Cl and Ca/Cl composition of the fluid inclusions could be influenced by seawater evaporation; however, intensive modification of K/Cl and Ca/Cl values caused by fluid-rock interactions during diagenesis is likely to account for large variation of K/Cl and Ca/Cl values. Illitisation of basin and basement rocks has been documented in the Athabasca Basin and is probably a major cause of K/Cl variation (Kister et al., 2006; Mercadier et al., 2010). Variations in formation water Ca/Cl are often attributed to either dolomitisation of limestones or albitisation of detrital plagioclase and basement rocks (Davisson and Criss, 1996; Houston et al., 2011). Detrital plagioclase are nearly absent from the preserved sedimentary succession (Ramaekers et al., 2007) and no albitisation of basement plagioclase is observed (Mercadier et al., 2010). However, stromatolitic to massive dolostones are described in the Carswell Formation (Ramaekers et al., 2007).

The range of U concentrations determined for fluid inclusions by *in vacuo* crushing in this study (3-169 ppm) is within the range of U concentrations (0.2-600 ppm) measured for individual inclusions by LA-ICP-MS (Richard et al., 2010, 2012). The U/Cl value is not correlated with either Ca/Cl or K/Cl (Fig. 5) or any other chemical parameter (e.g. Br/Cl and I/Cl; Table 2), suggesting NaCl and $CaCl_2$-rich fluid inclusions had comparable ranges of U concentration.

5.4. Origin of fluid inclusion excess ^{40}Ar.

The maximum $^{40}Ar/^{36}Ar$ values obtained for each sample (considered most representative of the brine inclusions), vary from 307 (RBL2Carb) to 460 (H3042-1) (Table 2). The range of $^{40}Ar/^{36}Ar$ is typical of upper crustal sedimentary formation waters and K-poor sedimentary rocks (Kendrick et al., 2002a,b; Ozima and Podosek, 2002; Kendrick and Burnard, 2013). The preserved sedimentary succession in the Athabasca Basin has a

maximum depositional age of 1.76 Ga and is characterised by a very low abundance of K (0.1-0.4 wt.%). In contrast, the Archean to Paleoproterozoic basement underlying the Athabasca Basin was >200 Ma old at the ~1.6-1.5 Ga time of mineralisation, and its much higher K content of 2-7 wt.% (Kister et al., 2006 and references therein) suggests it would have been an important reservoir of radiogenic ^{40}Ar at the time of mineralisation.

Deep percolation of the NaCl and $CaCl_2$-rich brines hundreds of meters below the basal unconformity of the Athabasca Basin, into the basement, is demonstrated by the intense alteration of the basement rocks into an illite-sudoite-dravite assemblage (Mercadier et al., 2010). Therefore, the basement is suggested as the most probable source of the excess ^{40}Ar component in the ore fluids.

However, basinal fluids could potentially have retained the relatively low, near atmospheric $^{40}Ar/^{36}Ar$ ratios of <450 (Fig. 6), during fluid interaction with the basement, if the amount of ^{40}Ar derived from the basement was small compared to the amount of atmospheric noble gas derived from eroded sedimentary material. Limited acquisition of ^{40}Ar is favoured by the low temperature of the fluids which is indicated to have been ~150 to ~200°C by fluid inclusion studies (Derome et al., 2005). The dominantly atmospheric origin of noble gases in solution is consistent with the subaerial origin of the brines, indicated by the halogen data, and it is in stark contrast to ore fluids with $^{40}Ar/^{36}Ar$ of >30,000 that were interpreted to have been derived from deep within Proterozoic basement lithologies in Australian ore deposits (Kendrick et al., 2011a,b).

5.5. Origin of fluid inclusion non-radiogenic isotopes (^{36}Ar, ^{84}Kr, ^{129}Xe) composition

The lowest calculated fluid inclusion ^{36}Ar concentration of 0.5×10^{-10} mol g^{-1} (Table 2) is slightly lower than that of modern air saturated meteoric water (0.7×10^{-10} mol g^{-1} at 0°C; Ozima and Podosek, 2002). However, it is considerably higher than calculated for a

brine formed by subaerial evaporation of seawater with 30 wt.% salts (bittern brine), which would have a ^{36}Ar concentration of only 0.07×10^{-10} mol g^{-1} at 25°C (Smith and Kennedy, 1983). The presence of 'excess ^{36}Ar', that is greater than can be explained by air saturation, could be partly explained if modern air contaminants trapped in empty fluid inclusions have mixed with noble gases in the fluid inclusions of our samples. However, we do not favour this as a major process because $F(^{129}Xe/^{36}Ar)_{air}$ is not strongly correlated with $^{40}Ar/^{36}Ar$, and all the fluid inclusion analyses have a range of $F(^{129}Xe/^{36}Ar)_{air}$ and $F(^{84}Kr/^{36}Ar)_{air}$ that are distinct from the composition of air (Fig. 6).

Higher than air-saturation ^{36}Ar concentrations and $F(^{129}Xe/^{36}Ar)_{air}$ and $F(^{84}Kr/^{36}Ar)_{air}$ intermediate of air and air-saturated water (Fig. 6) seem to be a real feature of many ore fluids (Kendrick et al., 2011c; Kendrick and Burnard, 2013). Considering ore fluids are chemically reactive solutions (as attested by alteration minerals, see Section 2.3), and atmospheric noble gases can have moderately high abundances in sedimentary rocks (see Table 3 in Podosek et al., 1980; Matsuda and Nagao, 1986; Matsubara et al., 1991; Matsuda and Matsubara, 1989; Ozima and Podosek, 2002), we suggest the fluid inclusions noble gas abundance pattern and high ^{36}Ar concentration could be explained by fluid interaction with sedimentary minerals. Atmospheric noble gases are adsorbed onto sedimentary materials during deposition, with a portion of the gases trapped in the mineral and a portion released to fluids during diagenesis (e.g. Podosek et al., 1980). Furthermore, atmospheric noble gases adsorbed onto sedimentary materials may be released to the fluid more easily than excess ^{40}Ar present inside mineral lattices. Therefore, we believe the measured $F(^{84}Kr/^{36}Ar)_{air}$ and $F(^{129}Xe/^{36}Ar)_{air}$ values could be fairly representative of NaCl and $CaCl_2$ fluid inclusions (and minor secondary fluid inclusions), and that these values can be explained by preferential acquisition of $^{36}Ar > ^{84}Kr > ^{129}Xe$ from the sedimentary rocks. The heavier noble gases (Xe and Kr) are even more enriched in sediments, than Ar, but are preferentially retained by the rock because they

have lower diffusion coefficients and higher adsorption coefficients (Ozima and Podosek, 2002).

5.6. Implications for uranium mineralisation

The mechanisms for reduction of U(VI) (the soluble form) to U(IV) and UO_2 deposition is one of the least understood aspects in the genesis of unconformity-related U deposits. Sangély et al. (2007) demonstrated much of the bitumen in these deposits has $\delta^{13}C$ of -31 to -49 ‰ that favours an inorganic origin and, together with petrographic observations, casts further doubt on the role of these organic materials. The local occurrence of co-precipitated UO_2 and bitumen has been used to suggest reduction of U(VI) by interaction between U-bearing brines and organic matter including bitumen with $\delta^{13}C$ of -26.8 ± 0.6 ‰ which may represent kerogen produced by cyanobacteria (Alexandre et al., 2006). It is not possible to exclude the possibility that organic matter could have been locally important for U reduction. However, the low I/Cl ratios of the U-related ore fluids from the four deposits included in this study indicate the brines investigated in this study have not interacted with biogenic organic matter.

The involvement of a basement-derived fluid has been suggested on the basis of stable (O, H) isotope composition of the alteration minerals such as illite, sudoite and dravite ($\delta^{18}O_{minerals}$ = 7 to 13 ‰ and $\delta D_{minerals}$ = -50 to -100 ‰; Wilson and Kyser 1987; Kotzer and Kyser 1995; Alexandre et al., 2005; Cloutier et al., 2009). These authors suggested mixing between a basement-derived (reducing) fluid and basin-derived brines could be responsible for part of the observed alteration and could have triggered UO_2 deposition. However, this view was recently challenged by O isotopic analysis of quartz and dolomite cements which points to isotopic equilibrium between the cement-forming fluids (i.e. NaCl- and $CaCl_2$-rich brines trapped as fluid inclusions) and the alteration minerals, meaning quartz and dolomite

cements as well as illite, sudoite and dravite may have formed from similar NaCl- and $CaCl_2$-rich brines (Richard et al., 2013b). The noble gas and halogen data presented in this study, suggest the fluid inclusions have an overwhelming origin (e.g. >90 %) from evolved basinal brines produced by subaerial evaporation of Proterozoic seawater. However, it is not possible to completely preclude the input of a volumetrically minor basement fluid (or gas), because if such a fluid had a low noble gas concentration and negligible salinity, its geochemical signature would be overwhelmed by the more voluminous saline fluids documented here.

Our favoured model for mineralisation is that interaction between brines and graphitic metapelites in the basement generated volumetrically minor mobile reductants, such as CH_4, H_2 or H_2S whose interaction with the brines could have triggered UO_2 deposition (Hoeve and Sibbald, 1978; Bray et al., 1988). The possibility also exists that deeply-sourced gases migrated along the faults controlling the U ore, these faults being deeply rooted in the graphitic metapelites (Györfi et al., 2007). Although direct evidence for such processes are currently lacking, such reactions are consistent with the presence of trace CH_4 and H_2 within fluid inclusions (Derome et al., 2003b) and the generally homogenous basinal signature of halogen and noble gas composition of the U-bearing brines documented in this study. Finally, the current dataset stresses the potential implication of fluid-gas interaction for localising the U deposition and encourages further experimental and analytical work on the origin and reactivity of such gases.

6. Conclusion

Analysis of noble gases (Ar, Kr, Xe) and halogens (Cl, Br, I) in U-rich NaCl- and $CaCl_2$-rich fluid inclusions from quartz and dolomite veins and breccia cements associated with alteration and mineralisation in four different Proterozoic unconformity-related U deposits in the Athabasca Basin suggest the following conclusions:

Halogen (Br/Cl and I/Cl) systematics demonstrate unambiguously that U-rich NaCl- and $CaCl_2$-rich brines (~25-35 wt.% salts) preserved in fluid inclusions formed by subaerial evaporation of seawater beyond the point of halite saturation. In contrast, the brines K/Cl and Ca/Cl ratios are largely rock-buffered.

The fluid inclusions have $^{40}Ar/^{36}Ar$ values that are only slightly higher than the modern atmospheric value. This is consistent with the halogen data and supports a subaerial origin from sedimentary formation waters. The fluid inclusions have higher ^{36}Ar, ^{84}Kr and ^{129}Xe concentrations than can be explained by air saturation, probably reflecting the acquisition of excess noble gases through interaction with clastic sediments that contained trapped atmospheric components. In contrast, the fluids acquired only minor excess ^{40}Ar during interaction with basement rocks.

Finally, the new data put further constraints on the mechanism of UO_2 deposition. The I/Cl data do not favour interaction between brines and organic matter as an important mechanism for precipitating U mineralisation. Together the halogen and noble gas data suggest the fluid inclusions are overwhelmingly dominated by fluids of a surficial origin and indicate that if a basement-derived fluid localised mineralisation it was volumetrically minor. We favour the hypothesis that a volumetrically minor gas phase with low noble gas and halogen concentration (e.g. CH_4, H_2 or H_2S) could have played an important role in localising U mineralisation.

Acknowledgements

This work was supported by a CNRS-GUTEC (Géologie de l'Uranium et du Thorium, Extraction, Conversion) grant. Dr Mark A. Kendrick is the recipient of an Australian Research Council QEII fellowship (Project number DP 0879451). Areva NC and Cameco are

also thanked for providing the samples and scientific collaboration as well as Julien Mercadier and Michel Cuney for fruitful discussions.

References

Alexandre, P., Kyser, K., Polito, P., Thomas, D. 2005. Alteration mineralogy and stable isotope geochemistry of Paleoproterozoic basement-hosted unconformity-type uranium deposits in the Athabasca Basin, Canada. Economic Geology 100, 1547–1563.

Alexandre, P., Kyser, T. K. 2006. Geochemistry of uraniferous bitumen in the Southwest Athabasca basin, Saskatchewan, Canada. Economic Geology 101, 1605–1612.

Alexandre, P., Kyser K., Thomas, D., Polito, P., Marlat, J. 2009. Geochronology of unconformity-related uranium deposits in the Athabasca Basin, Saskatchewan, Canada and their integration in the evolution of the basin. Mineralium Deposita 44, 41–59.

Annesley, I.R., Madore, C., Portella, P. 2005. Geology and thermotectonic evolution of the western margin of the Trans-Hudson Orogen: Evidence from the eastern sub-Athabasca basement, Saskatchewan. Canadian Journal of Earth Sciences 42, 573–597.

Ballentine, C.J., Burnard P.G. 2002. Production, release and transport of noble gases in the continental crust. In: Porcelli, D., Ballentine, C.J., Wieler, R. (Eds.), Noble Gases in Geochemistry and Cosmochemistry. Reviews in Mineralogy and Geochemistry 47, 481–538.

Banks, D.A., Guiliani, G., Yardley, B.W.D., Cheilletz, A., 2000. Emerald mineralization in Colombia: fluid chemistry and the role of brine mixing. Mineralium Deposita 35, 699–713.

Beyer, S.R, Hiatt, E.E., Kyser, K., Dalrymple, R.W., Pettman, C., 2011. Hydrogeology, sequence stratigraphy and diagenesis in the Paleoproterozoic western Thelon Basin:

Influences on unconformity-related uranium mineralization. Precambrian Research 187, 293–312.

Böhlke, J.K., Irwin, J.J. 1992a. Brine history indicated by argon, krypton, chlorine, bromine, and iodine analyses of fluid inclusions from the Mississippi Valley type lead-fluorite-barite deposits at Hansonburg, New Mexico. Earth Planetary Science Letters 110, 51–66.

Böhlke, J.K., Irwin, J.J. 1992b. Laser microprobe analyses of Cl, Br, I and K in fluid inclusions: Implications for sources of salinity in some ancient hydrothermal fluids. Geochimica et Cosmochimica Acta 56, 203–225.

Boiron, M.C., Cathelineau, M., Richard, A., 2010. Fluid flows and metal deposition near basement / cover unconformity: Lessons and analogies from Pb-Zn-F-Ba systems for the understanding of Proterozoic U deposits. Geofluids 10, 270–292.

Bray, C.J., Spooner, E.T.C., Longstaffe, F.J., 1988. Unconformity-related uranium mineralization, McClean deposits, North Saskatchewan, Canada: Hydrogen and oxygen isotope geochemistry. Canadian Mineralogist 26, 249–268.

Card, C.D., Pana, D., Portella, P., Thomas, D.J., Annesley, I.R., 2007. Basement rocks to the Athabasca Basin, Saskatchewan and Alberta. In: Jefferson, C.W., Delaney, G. (Eds.), EXTECH IV: Geology and Uranium EXploration TECHnology of the Proterozoic Athabasca Basin, Saskatchewan and Alberta. Geological Survey of Canada Bulletin 588, 69–87.

Chiarenzelli, J., Aspler, L., Villeneuve, M., Lewry, J., 1998. Early Proterozoic evolution of the Saskatchewan craton and its allochtonous cover, Trans-Hudson orogen. Journal of Geology 106, 247–267.

Cloutier, J., Kyser, K., Olivo, G.R., Alexandre, P., Halaburda, J., 2009. The Millennium uranium deposit, Athabasca Basin, Saskatchewan, Canada: An atypical basement-hosted unconformity-related uranium deposit. Economic Geology 104, 815–840.

Cloutier, J., Kyser, K., Olivo, G., Brisbin, D., 2011. Geochemical, isotopic, and geochronologic constraints on the formation of the Eagle Point basement-hosted uranium deposit, Athabasca Basin, Saskatchewan, Canada and recent remobilization of primary uraninite in secondary structures. Mineralium Deposita 46, 35–56.

Cumming, G.L., Krstic, D., 1992. The age of unconformity-related uranium mineralization in the Athabasca Basin, Northern Saskatchewan. Canadian Journal of Earth Sciences 29, 1623–1639.

Cuney, M., 2010. Evolution of uranium fractionation processes through time: Driving the secular variation of uranium deposit types. Economic Geology 105, 553–569.

Dahlkamp, F.J., 1978. Geologic appraisal of the Key Lake U-Ni deposits, northern Saskatchewan: Economic Geology 73, 1430–1449.

Davisson, M.L., Criss, R.E., 1996. Na-Ca-Cl relations in basinal fluids. Geochimica et Cosmochimica Acta 60, 2743–2752.

Derome, D., Cuney, M., Cathelineau, M., Fabre, C., Dubessy, J., Bruneton, P., Hubert, A., 2003a. A detailed fluid inclusion study in silicified breccias from the Kombolgie sandstones (Northern Territory, Australia): inferences for the genesis of middle-Proterozoic unconformity-type uranium deposits. Journal of Geochemical Exploration 80, 259–275.

Derome D., Cathelineau, M., Lhomme, T., Cuney, M., 2003b. Fluid inclusion evidence of the differential migration of H_2 and O_2 in the McArthur River unconformity-type uranium deposit (Saskatchewan, Canada). Possible role on post-ore modifications of the host rocks. Journal of Geochemical Exploration 78–79, 525–530.

Derome, D., Cathelineau, M., Cuney, M., Fabre, C., Lhomme, T., Banks, D.A., 2005. Mixing of sodic and calcic brines and uranium deposition at McArthur River, Saskatchewan, Canada: A Raman and laser-induced breakdown spectroscopic study of fluid inclusions. Economic Geology 100, 1529–1545.

Derome, D., Cathelineau, M., Fabre, C., Boiron, M.C., Banks, D., Lhomme T., Cuney, M., 2007. Paleo-fluid composition determined from individual fluid inclusions by Raman and LIBS: Application to mid-proterozoic evaporitic Na-Ca brines (Alligator Rivers Uranium Field, northern territories Australia). Chemical Geology 237, 240–254.

Fayek, M., Kyser, T.K., 1997. Characterization of multiple fluid-flow events and rare-earth-element mobility associated with formation of unconformity-type uranium deposits in the Athabasca Basin, Saskatchewan. Canadian Mineralogist 35, 627–658.

Fayek, M., Kyser, T.K., Riciputi, L.R., 2002. U and Pb isotope analysis of uranium minerals by ion microprobe and the geochronology of McArthur River and Sue Zone uranium deposits, Saskatchewan, Canada. Canadian Mineralogist 40, 1553–1569.

Fehn, U., Lu, Z., Tomaru, H., 2006. ^{129}I/I ratios and halogen concentrations in pore water of Hydrate Ridge and their relevance for the origin of gas hydrates: A progress report. In: Tréhu, A.M., Bohrmann, G., Torres, M.E., Colwell, F.S. (Eds.), Proceedings of the Ocean Drilling Program, Scientific Results, 1–25.

Fisher, L.A., Kendrick, M.A., 2008. Metamorphic fluid origins in the Osborne Fe oxide–Cu–Au deposit, Australia: evidence from noble gases and halogens. Mineralium Deposita 43, 483–497.

Fontes, J.C., Matray, J.M., 1993. Geochemistry and origin of formation brines from the Paris Basin, France 1. Brines associated with Triassic salts. Chemical Geology 109, 149–175.

Gaboreau S., Cuney M., Quirt D., Beaufort D., Patrier P. and Mathieu R., 2007. Significance of aluminum phosphate-sulfate minerals associated with U unconformity-type deposits: The Athabasca basin, Canada. American Mineralogist 92, 267–280.

Györfi, I., Hajnal, Z., White, D.J., Takacz, E., Reilkoff, B., Annesley, I.R., Powell, B., Koch, R., 2007. High resolution seismic survey from the McArthur River region: contribution to mapping of the P2 uranium ore zone, Athabasca Basin, Saskatchewan. In: Jefferson, C.W., Delaney, G. (Eds.), EXTECH IV: Geology and Uranium EXploration TECHnology of the Proterozoic Athabasca Basin, Saskatchewan and Alberta. Geological Survey of Canada Bulletin 588, 397–412.

Hammerli, J., Rusk, B., Spandler, C., Emsbo, P., Oliver, N.H.S., 2013. In situ quantification of Br and Cl in minerals and fluid inclusions by LA-ICP-MS: A powerful tool to identify fluid sources. Chemical Geology 337–338, 75–87.

Houston, S., Smalley, C., Laycock, A., Yardley, B.W.D., 2011. The relative importance of buffering and brine inputs in controlling the abundance of Na and Ca in sedimentary formation waters. Marine and Petroleum Geology 28, 1242–1251.

Hardie, L.A., 2003. Secular variations in Precambrian seawater chemistry and the timing of Precambrian aragonite seas and calcite seas. Geology 31, 785–788.

Hecht, L., Cuney, M., 2000. Hydrothermal alternation of monazite in the Precambrian crystalline basement of the Athabasca Basin (Saskatchewan, Canada): Implications for the formation of unconformity-related uranium deposits. Mineralium Deposita 35, 791–795.

Heine, T. H., 1986. The geology of the Rabbit Lake uranium deposit, Saskatchewan. In: Evans, E.L. (Ed.), Uranium Deposits of Canada. Canadian Institute of Mining, Metallurgy and Petroleum, Special Volume 33, 134–143.

Hoeve, J., Sibbald, T.I.I., 1978. On the genesis of the Rabbit Lake and other unconformity-type uranium deposits in Northern Saskatchewan, Canada. Economic Geology 73, 1450–1473.

Hoffman, P.F., 1990. Subdivision of the Churchill Province and extent of the Trans-Hudson Orogen. In: Lewry, J.F., Stauffer, M.R. (Eds.), The Early Proterozoic Trans-Hudson Orogen of North America. Geological Association of Canada Special Paper 37, 15–39.

Holser, W.T., 1979. Trace elements and isotopes in evaporates. In: Burns, R.G. (Ed.), Marine Minerals. Reviews in Mineralogy 6, 295–346.

Hu, R.Z., Burnard, P.G., Bi, X.W.,, Zhou, M.F., Peng, J.T., Su, W.C., Zhao, J.H., 2009. Mantle-derived gaseous components in ore-forming fluids of the Xiangshan uranium deposit, Jiangxi province, China: Evidence from He, Ar and C isotopes. Chemical Geology 266, 86–95.

Jefferson, C.W., Thomas, D.J., Gandhi, S.S., Ramaekers, P., Delaney, G., Brisbin, D., Cutts, C., Portella, P., Olson, R.A., 2007. Unconformity associated uranium deposits of the Athabasca Basin, Saskatchewan and Alberta. In: Jefferson, C.W., Delaney, G. (Eds.), EXTECH IV: Geology and Uranium EXploration TECHnology of the Proterozoic Athabasca Basin, Saskatchewan and Alberta. Geological Survey of Canada Bulletin 588, 23–67.

Johnson, L.H., Burgess, R., Turner, G., Milledge, H.J., Harris, J.W., 2000. Noble gas and halogen geochemistry of mantle fluids: Comparison of African and Canadian diamonds. Geochimica et Cosmochimica Acta 64, 717–732.

Kendrick, M.A., Burgess, R., Pattrick, R.A.D., Turner, G., 2001. Noble gas and halogen evidence on the origin of Cu-Porphyry mineralising fluids. Geochimica et Cosmochimica Acta 65, 2651–2668.

Kendrick, M.A., Burgess, R., Leach, D., Pattrick, R.A.D., 2002a. Hydrothermal fluid origins in Mississippi Valley-type ore districts: Combined noble gas (He, Ar, Kr) and halogen (Cl, Br, I) analysis of fluid inclusions from the Illinois-Kentucky fluorspar district, Viburnum Trend, and Tri-State districts, midcontinent United States. Economic Geology 97, 453–469.

Kendrick, M.A., Burgess, R., Pattrick, R.A.D., Turner, G., 2002b. Hydrothermal fluid origins in a fluorite-rich Mississippi Valley-type district: Combined noble gas (He, Ar, Kr) and halogen (Cl, Br, I) analysis of fluid inclusions from the South Pennine ore field, United Kingdom. Economic Geology 97, 435–451.

Kendrick, M.A., Duncan, R.J., Phillips, D., 2006. Noble gas and halogen constraints on mineralizing fluids of metamorphic versus surficial origin: Mt Isa Australia. Chemical Geology 235, 325–351.

Kendrick, M.A., Mark, G., Phillips, D., 2007. Mid-crustal fluid mixing in a Proterozoic Fe oxide-Cu-Au deposit, Ernest Henry, Australia: Evidence from Ar, Kr, Xe, Cl, Br and I. Earth Planetary Science Letters 256, 328–343.

Kendrick, M.A., Phillips, D., 2009. New constraints on the release of noble gases during in vacuo crushing and application to scapolite Br-Cl-I and $^{40}Ar/^{39}Ar$ age determinations: Geochimica et Cosmochimica Acta 73, 5673–5692.

Kendrick, M.A., Honda, M., Oliver, N.H.S., Philipps, D. 2011a. The noble gas systematics of late-orogenic H_2O-CO_2 fluids, Mt Isa, Australia. Geochimica et Cosmochimica Acta 75, 1428–1450.

Kendrick, M.A., Honda, M., Walshe, J., Petersen, K., 2011b. Fluid sources and the role of abiogenic-CH_4 in Archean gold mineralization: Constraints from noble gases and halogens. Precambrian Research 189, 313–327.

Kendrick, M.A., Phillips, D., Wallace, M., Miller, J.McL., 2011c. Halogens and noble gases in sedimentary formation waters and Zn–Pb deposits: A case study from the Lennard Shelf, Australia. Applied Geochemistry 26, 2089–2100.

Kendrick, M.A., 2012. High precision Cl, Br and I determinations in mineral standards using the noble gas method. Chemical Geology 292–293, 116–126.

Kendrick, M.A., Arculus, R., Burnard, P., Honda, M., 2013. Quantifying brine assimilation by submarine magmas: Examples from the Galápagos Spreading Centre and Lau Basin. Earth and Planetary Science Letters 365, 86–96. Geochimica et Cosmochimica Acta 123, 150-165.

Kendrick, M.A., Burnard, P., 2013. Noble gases and halogens in fluid inclusions: A journey through the Earth's crust. In: Burnard, P. (Ed.), The Noble Gases as Geochemical Tracers. Springer-Verlag, Berlin, 319–369.

Kister, P., Laverret, E., Quirt, D., Cuney, M., Patrier Mas, P., Beaufor,t D., Bruneton, P., 2006. Mineralogy and geochemistry of the host-rock alterations associated with the Shea Creek unconformity-type uranium deposits (Athabasca basin, Saskatchewan, Canada). Part 2. Regional-scale spatial distribution of the Athabasca Group sandstone matrix minerals. Clays and Clay minerals 54, 295–313.

Kotzer, T.G., Kyser, T.K., 1995. Petrogenesis of the Proterozoic Athabasca Basin, Northern Saskatchewan, Canada, and its relation to diagenesis, hydrothermal uranium mineralization and paleohydrogeology. Chemical Geology 120, 45–89.

Kovalevych, V., Marshall, T., Peryt, T.M., Petrychenko, O.Y., Zhukova, S.A., 2006. Chemical composition of seawater in Neoproterozoic: Results of fluid inclusion study of halite from Salt Range (Pakistan) and Amadeus Basin (Australia). Precambrian Research 144, 39–51.

Kyser, T.K., Hiatt, E., Renac, C., Durocher, K., Holk, G., Deckart, K., 2000. Diagenetic fluids in paleo- and meso-proterozoic sedimentary basins and their implications for long protracted fluid histories. In: Kyser, K. (Ed.), Fluids and Basin Evolution. Mineralogical Association of Canada Short Course Series 28, 225–262.

Kyser, T.K., Cuney, M., 2008. Unconformity-related uranium deposits. In: Cuney, M., Kyser, K. (Eds.), Recent and Not-So-Recent Developments in Uranium Deposits and Implications for Exploration. Mineralogical Association of Canada Short Course Series 39, 161–219.

Leisen, M., Boiron, M.C., Richard, A., Dubessy, J., 2012. Determination of Cl and Br concentrations in individual fluid inclusions by combining microthermometry and LA-ICPMS analysis: Implications for the origin of salinity in crustal fluids. Chemical Geology 330–331, 197–206.

Lorilleux, G., Jébrak, M., Cuney, M., Baudemont, D., 2002. Polyphase hydrothermal breccia associated with unconformity-related uranium mineralizations (Canada). From fractal analysis to structural significance. Journal of Structural Geology 24, 323–338.

Lorilleux, G., Cuney, M., Jébrak, M., Rippert, J.C., Portella, P., 2003. Chemical brecciation processes in the Sue unconformity-type uranium deposits, Eastern Athabasca Basin (Canada). Journal of Geochemical Exploration 80, 241–258.

Lowenstein, T.K., Timofeeff, M.N., Brennan, S.T., Hardie, L.A., Demicco, R.V., 2001. Oscillations in Phanerozoic seawater chemistry: Evidence from fluid inclusions. Science 294, 1086–1088.

Lowenstein, T.K., Timofeeff, M.N., 2008. Secular variations in seawater chemistry as a control on the chemistry of basinal brines: test of the hypothesis. Geofluids 8, 77–92.

Mathieu, R, Cuney, M, Cathelineau, M., 2000. Geochemistry of paleofluids circulation in the Franceville basin and around Olko natural reaction zones (Gabon). Journal of Geochemical Exploration 69–70, 245–249.

Matsubara, K., Matsuda, J., Sugisaki, R., 1991. Noble gases in mesozoic cherts from the USA and Japan. Chemical Geology 86, 287–293.

Matsuda, J., Nagao, K., 1986. Noble-gas abundances in a deep-sea sediment core from eastern equatorial Pacific. Geochemical Journal 20, 71–80.

Matsuda, J., Matsubara, K., 1989. Noble-gases in silica and their implication for the terrestrial missing Xe. Geophysical Research Letters 16, 81–84.

Mercadier, J., Richard, A., Boiron, M.C., Cathelineau, M., Cuney, M., 2010. Brine migration in the basement rocks of the Athabasca Basin through microfracture networks (P-Patch U deposit, Canada). Lithos 115, 121–136.

Mercadier, J., Cuney, M., Lach, P., Boiron, M.C., Bonhoure, J., Richard, A., Leisen, M., Kister, P., 2011a. Origin of uranium deposits revealed by their rare earth element signature. Terra Nova 23, 264–269.

Mercadier, J., Cuney, M., Cathelineau, M., Lacorde, M., 2011b. U redox fronts and kaolinisation in basement-hosted unconformity-related U ores of the Athabasca Basin (Canada): late U remobilisation by meteoric fluids. Mineralium Deposita 46, 105–135.

Mercadier, J., Richard, A., Cathelineau, M. 2012. Boron and magnesium-rich marine brines at the origin of giant unconformity-related uranium deposits: $\delta^{11}B$ evidence from Mg-tourmalines. Geology 40, 231–234.

Mercadier, J., Annesley, I.R., McKechnie, C.L., Bogdan, T., Creighton, S., 2013. Magmatic and metamorphic uraninite mineralization in the western margin of the Trans-Hudson Orogen (Saskatchewan, Canada): a metal source for unconformity-related uranium deposits? Economic Geology 108, 1037–1065.

Meshik, A.P., Hohenberg, C.M., Pravdivtseva, O.V., 2004. Record of cycling operation of the natural nuclear reactor in the Oklo/Okelobondo area in Gabon. Physical Review Letters 93, 182–302.

Muramatsu, Y., Doi, T., Tomaru, H., Fehn, U., Takeuchi, R., Matsumoto, R., 2007. Halogen concentrations in pore waters and sediments of the Nankai Trough, Japan: Implications for the origin of gas hydrates. Applied Geochemistry 22, 534–556.

Ng, R., Alexandre, P., Kyser, K., 2013. Mineralogical and geochemical evolution of the unconformity-related McArthur River Zone 4 orebody in the Athabasca Basin, Canada: Implications of a silicified zone. Economic Geology 108, 1657–1689.

Nissenbaum A. (1977) Minor and trace elements in Dead Sea water. Chemical Geology 19, 99–111.

Ozima, M., Podosek, F.A., 2002. Noble Gas Geochemistry. Cambridge University Press.

Pagel, M., 1975. Détermination des conditions physico-chimiques de la silicification diagénétique des grès Athabasca (Canada) au moyen des inclusions fluides. Comptes Rendus de l'Académie des Sciences de Paris 280(D), 2301–2304.

Pagel, M., Jaffrezic, H. 1977. Analyses chimiques des saumures des inclusions du quartz et de la dolomite du gisement d'uranium de Rabbit Lake (Canada). Aspect méthodologique et importance génétique. Comptes Rendus de l'Académie des Sciences 284(D), 113–116.

Pagel, M., Poty, B., Sheppard, S.M.F., 1980. Contribution to some Saskatchewan uranium deposits mainly from fluid inclusion and isotopic data. In: IAEA (Ed.), International Uranium Symposium on the Pine Creek Geosyncline, Vienna, 639–654.

Podosek, F.A., Honda, M., Ozima, M., 1980. Sedimentary noble gases. Geochimica et Cosmochimica Acta 44, 1875–1884.

Polito, P.A., Kyser, T.K., Alexandre, P., Hiatt, E.E., Stanley, C.R., 2011. Advances in understanding the Kombolgie Subgroup and unconformity-related uranium deposits in the Alligator Rivers Uranium Field and how to explore for them using lithogeochemical principles. Australian Journal of Earth Sciences 58, 453–474.

Ramaekers, P., Jefferson, C.W., Yeo, G.M., Collier, B., Long, D.G., Catuneanu, O., Bernier, S., Kupsch, B., Post, R., Drever, G., McHardy, S., Jircka, D., Cutts, C., Wheatley, K., 2007. Revised geological map and stratigraphy of the Athabasca Group, Saskatchewan and Alberta. In: Jefferson, C.W., Delaney, G. (Eds.), EXTECH IV: Geology and Uranium EXploration TECHnology of the Proterozoic Athabasca Basin, Saskatchewan and Alberta. Geological Survey of Canada Bulletin 588, 155–578.

Renac, C., Kyser, T.K., Durocher, K., Dreaver, G., O'Connor, T., 2002. Comparison of diagenetic fluids in the Proterozoic Thelon and Athabasca Basins, Canada: implications for protracted fluid histories in stable intracratonic basins. Canadian Journal of Earth Sciences 39, 113–132.

Richard, A., Pettke, T., Cathelineau, M., Boiron, M.C., Mercadier, J., Cuney, M., Derome, D., 2010. Brine-rock interaction in the Athabasca basement (McArthur River U deposit, Canada): consequences for fluid chemistry and uranium uptake. Terra Nova 22, 303–308.

Richard, A., Banks, D.A., Mercadier, J., Boiron, M.C., Cuney, M., Cathelineau, M., 2011. An evaporated seawater origin for the ore-forming brines in unconformity-related uranium deposits (Athabasca Basin, Canada): Cl/Br and δ^{37}Cl study of fluid inclusions. Geochimica et Cosmochimica Acta 75, 2792–2810.

Richard, A, Rozsypal, C., Mercadier, J., Banks, D.A., Cuney, M., Boiron, M.C., Cathelineau, M., 2012. Giant uranium deposits formed from exceptionally uranium-rich acidic brines. Nature Geoscience 5, 142–146.

Richard, A., Cauzid J., Cathelineau M., Boiron M.C., Mercadier J., Cuney, M., 2013a. Synchrotron-XRF and XANES investigation of uranium speciation and element distribution in fluid inclusions from unconformity-related uranium deposits. Geofluids, 13, 101–111.

Richard, A., Boulvais, P., Mercadier, J., Boiron, M.C., Cathelineau, M., Cuney, M., 2013b. From evaporated seawater to uranium-mineralizing brines: Isotopic and trace element study of quartz-dolomite veins in the Athabasca system. Geochimica et Cosmochimica Acta 113, 38–59.

Sangély, L., Chaussidon, M., Michels, R., Brouand, M., Cuney, M., Huault, V., Landais, P., 2007. Micrometer scale carbon isotopic study of bitumen associated with Athabasca uranium deposits: Constraints on the genetic relationship with petroleum source-rocks and the abiogenic origin hypothesis. Earth and Planetary Science Letters 258, 378–396.

Shukolyukov, Y.A., Ashkinadze, G.S., Verkhovskii, A.B. 1976. Anomalous isotope composition of xenon and krypton in minerals of the natural nuclear reactor. Atomic Energy 41, 663–666.

Smith, S.P., Kennedy, B.M., 1983. The solubility of noble gases in water and in NaCl brine. Geochimica et Cosmochimica Acta 47, 503–515.

Wilson, M.R., Kyser, T.K., 1987. Stable isotope geochemistry of alteration associated with the Key Lake uranium deposit, Canada. Economic Geology 82, 1540–1557.

Zherebtsova, I.K., Volkova, N.N., 1966. Experimental study of behaviour of trace elements in the process of natural solar evaporation of Black Sea water and Lake Sasky-Sivash brine. Geochemistry International 3, 656–670.

Table captions

Table 1: Location, petrography and fluid inclusion mean salinity (± 2σ) of the studied samples. U/C: unconformity; FI: fluid inclusions; *N*: number fluid inclusions analysed per sample by microthermometry. Only brine inclusions were considered (not scarce low-salinity secondary inclusions). Following the nomenclature in Derome et al. (2005), inclusions showing a halite cube at room temperature are noted Lwh' or Lwh according to the nature of their last phase to melt (ice or hydrohalite respectively) during low temperature microthermometric runs and according to their mode of homogenization (by halite or vapor disappearance respectively). Inclusions with no halite cube whose last phase to melt is hydrohalite are noted Lw2. Inclusions with no halite cube whose last phase to melt is ice are noted Lw' (-60°C < *Tm ice* < -30°C), or Lw1 (-30°C < *Tm ice* < -15°C), where *Tm ice* is the temperature for ice melting. Mineral abbreviations: Qtz: quartz; Dol: dolomite; Su: sudoite; Hem: haematite; Drv: dravite. "bleached" stands for samples altered to illite-sudoite-dravite±quartz assemblages.

Table 2: Summary of fluid inclusion noble gas, halogen and cation data for quartz and dolomite samples in unconformity-related uranium deposits, (Athabasca Basin), determined by *in vacuo* crushing. All ratios are molar. $^{40}Ar_E$: age-corrected excess ^{40}Ar ($^{40}Ar_E = {}^{40}Ar_{total} - {}^{40}Ar_R - {}^{40}Ar_A$), $^{40}Ar_R$: radiogenic ^{40}Ar produced in situ since 1.6 Ga., $^{40}Ar_A$: atmospheric $^{40}Ar = 296 \times {}^{36}Ar$. Representative Ar concentrations have been calculated from mean salinity (Table 1). Fluid inclusion $F(^{84}Kr/^{36}Ar)_{air}$ versus $F(^{129}Xe/^{36}Ar)_{air}$ are defined as $F(X/^{36}Ar)_{air} = (X/^{36}Ar)_{sample}/(X/^{36}Ar)_{air}$; reference values for air from Ozima and Podosek (2002). nd.: not determined. dupl.: duplicate analysis.

* These samples have age-corrected (1.6 Ga) $^{40}Ar/^{36}Ar$ values lower than the modern atmosphere value of 296, meaning $^{40}Ar_E/Cl$ and $[^{40}Ar_E]$ values cannot be calculated for these data.

Table 3: Summary of fluid inclusion noble gas, halogen and cation data for quartz and dolomite samples in unconformity-related uranium deposits, (Athabasca Basin), determined by fusion. All ratios are molar. $^{40}Ar_E$: age-corrected excess ^{40}Ar ($^{40}Ar_E = {}^{40}Ar_{total} - {}^{40}Ar_R - {}^{40}Ar_A$), $^{40}Ar_R$: radiogenic ^{40}Ar produced in situ since 1.6 Ga., $^{40}Ar_A$: atmospheric $^{40}Ar = 296 \times {}^{36}Ar$. Fluid inclusion $F(^{84}Kr/^{36}Ar)_{air}$ versus $F(^{129}Xe/^{36}Ar)_{air}$ are defined as $F(X/^{36}Ar)_{air} = (X/^{36}Ar)_{sample}/(X/^{36}Ar)_{air}$; reference values for air from Ozima and Podosek (2002). * Sample ES287-10 has K/Cl of ~6.5 meaning fusion released a lot of K and Ar from mineral impurities (see Section 4) and the age-corrected (1.6 Ga) $^{40}Ar/^{36}Ar$ cannot be calculated. ** Sample H3042-1 has a measured $^{40}Ar/^{36}Ar$ of 291, lower than the modern atmosphere value of 296, meaning an age cannot be calculated.

Figure captions

Figure 1: (A) Simplified geological map of the Athabasca Basin and its underlying basement, with location of the four studied unconformity-related U deposits (modified from Jefferson et al., 2007 and Card et al., 2007). WMTZ: Wollaston-Mudjatik transition zone. (B) Simplified mineral paragenesis for unconformity-related U deposits in the Athabasca Basin. The types of alteration (E: early diagenetic, hydrothermal and late meteoric), are indicated. Hydrothermal alteration and mineralisation spanned a period of <150 Ma between 1670 and 1500 Ma (see Section 2.3. for details) and late meteoric

events are indicated to be younger than 400 Ma (Mercadier et al., 2011b).The alteration assemblage contemporaneous of the primary U mineralisation is composed of, illite, sudoite (Mg-chlorite), dravite (Mg-tourmaline), euhedral quartz, dolomite, haematite and bitumen. Compac.: compaction ; Diag.: diagenetic. APS: aluminium phosphate-sulphate (APS) minerals. Modified from Kotzer and Kyser (1995), Derome et al., (2005), Kyser and Cuney (2008) and Mercadier et al. (2012).

Figure 2: Examples of quartz and dolomite veins and breccia cements, hosting fluid inclusions studied in this work. (A) Quartz vein crosscutting "bleached" gneiss (sample P48-5, P-Patch deposit). (B) Dravite + quartz cementing vein in graphite-rich gneiss (samples H3042-1, Eagle point Deposit). (C) Quartz and dolomite cementing vein crosscutting a haematite-rich gneiss (sample RBL2, Rabbit Lake deposit). (D) Typical primary two-phase (liquid + vapor) fluid inclusions in quartz. (E) Typical three-phase (liquid-vapor-halite) fluid inclusions in quartz. Note that similar two-phase and three phase inclusions were found in both quartz and dolomite. Abbreviations: Qtz: quartz; Dol: dolomite; Hem: haematite; Drv: dravite; Liq: liquid; Vap: vapour; Hal: halite. Further illustration of fluid inclusions and quartz and dolomite veins and breccia cements from McArthur River, Rabbit Lake, P-Patch and Eagle Point deposits, can be found in Pagel et al., 1980; Kotzer and Kyser, 1995; Derome et al., 2005; Richard et al., 2010, 2011, 2012, 2013a).

Figure 3: (A) Fluid inclusion Br/Cl versus I/Cl molar ratios determined by *in vacuo* crushing. Typical 1σ internal uncertainties on Br/Cl and I/Cl values lie within the size of symbols. The composition of the seawater evaporation trajectory (SET); halite; fluids that dissolve evaporites; marine pore fluids; mid-continent MVT and magmatic fluids

are based on Zherebstova and Volkova, (1966); Holser (1979); Böhlke and Irwin (1992b); Banks et al. (2000); Kendrick et al. (2001; 2002; 2011c); Fehn et al. (2006); Muramatsu et al. (2007); the complete list of references for all fields are given in Kendrick and Burnard (2013). Marine pore fluids are characterised by organic Br and I. Assuming an initial seawater Br/Cl value, most marine pore fluids acquire organic Br and I in a ratio of 0.5–2.5 (Kendrick et al., 2011c). (B) Fluid inclusion Br/Cl versus Cl concentration determined by *in vacuo* crushing. Br/Cl values are the average Br/Cl among successive extractions for each sample (error bars indicate minimum and maximum values). Cl concentrations have been deduced from the mean salinity (± 2σ) of the studied samples (as expressed in wt.% eq. NaCl). SET: seawater evaporation trajectory after Fontes and Matray (1993). Minerals precipitating during evaporation of seawater: G: gypsum, H: halite, E: epsomite, S: sylvite, C: carnallite, B: bischofite. (C) Comparison between average Br/Cl values determined in this study by *in vacuo* crushing (full symbols) and fusion (crossed full symbol symbols), and Br/Cl values obtained on the same samples by crush-leach and ion chromatography (Richard et al., 2011).

Figure 4: Fluid inclusion K/Cl versus Ca/Cl molar ratios determined by *in vacuo* crushing. The approximate fields for NaCl-rich and $CaCl_2$-rich fluid inclusion end-members are shown for comparison, based on K, Ca (and other cations) determination from LA-ICP-MS analyses and Cl determination from microthermometry (Richard et al., 2010; Derome et al., 2005).

Figure 5: (A) Fluid inclusion K/Cl versus Br/Cl molar ratios determined by *in vacuo* crushing. (B) Fluid inclusion Ca/Cl versus Br/Cl molar ratios determined by *in vacuo* crushing.

Table 1

Sample	Depth below U/C (m)	Description	FI frequencies						FI relative abundances (%)		Salinity	± 2σ
			NaCl-rich			$CaCl_2$-rich		*N*	NaCl-rich	$CaCl_2$-rich	mean	(%)
			Lw1	Lw2	Lwh	Lw'	Lwh'				(wt% eq. NaCl)	
Eagle Point deposit - Quartz												
ES287-10	259	Qtz vein in bleached pelitic gneiss	6	17	0	0	0	23	100	0	28.5	10
H3042-1	263	Qtz+drv vein in graphite-rich gneiss	2	5	0	15	7	29	24	76	30.3	25
P-Patch deposit - Quartz												
P48-2	39	Qtz vein in chloritised gneiss	1	14	0	7	4	26	58	42	29.9	15
P48-5	52	Qtz vein in bleached gneiss	3	4	0	12	1	20	35	65	27.0	15
McArthur River deposit - Quartz												
MAC54Qz	50	Qtz+drv+sulfides cement in Su-rich breccia	0	47	7	0	0	54	100	0	27.5	10
Rabbit Lake deposit - Quartz												
RBL2Qz	*	Qtz+dol vein in hem-rich gneiss	1	46	0	0	0	47	100	0	29.2	10
RBL7Qz	*	Qtz+dol cement in hydraulic megabreccia	0	5	0	2	2	9	56	44	28.9	30
Rabbit Lake deposit - Dolomite												
RBL2Carb	*	Qtz+dol vein in hem-rich gneiss	14	25	0	0	0	39	100	0	27.6	5
RBL7Carb	*	Qtz+dol cement in hydraulic megabreccia	1	12	0	2	0	15	87	13	28.1	10

Table 2

Sample name	Sample weight (mg)	Extraction	Cl mol g^{-1} (×10^{-6})	Br/Cl (×10^{-3})	±	I/Cl (×10^{-6})	±	K/Cl	±	Ca/Cl	±	U/Cl	[U] ppm	^{36}Ar mol g^{-1} (×10^{-14})	Age Ma	±	^{40}Ar/^{36}Ar Measured	±	^{40}Ar/^{36}Ar (1.6 Ga)	±	F(^{84}Kr/^{36}Ar)$_{air}$	±	F(^{129}Xe/^{36}Ar)$_{air}$	±	Cl/^{36}Ar (×10^{6})	±	^{40}Ar$_E$/Cl (×10^{-6}) (1.6 Ga)	±	[^{36}Ar] mol g^{-1} (×10^{-10})	[^{40}Ar$_E$] mol g^{-1} (×10^{-8}) (1.6 Ga)
Eagle Point deposit - Quartz																															
ES287-10	88.7	cr #1	1.3	7.6	0.2	2.0	0.1	0.033	0.002	0.08	0.02	nd		5.5	3436	719	350	4	337	4	1.04	0.04	1.19	0.05	23.2	0.3	1.8	0.2	2.1	0.9
	88.7	cr #2	0.6	7.3	0.2	1.9	0.1	0.038	0.001	nd		7.8E-06	9	1.0	3581	865	467	25	428	23	1.20	0.08	1.64	0.19	58.2	3.1	2.3	0.3	0.8	1.1
ES287-10 (dupl.)	49.4	cr #1	1.3	7.3	0.2	2.4	0.1	0.056	0.004	nd		nd		5.7	3137	712	369	7	347	7	1.05	0.05	1.35	0.09	22.4	0.5	2.3	0.3	2.2	1.1
H3042-1	95.4	cr #1	1.4	10.4	0.1	2.3	0.1	0.026	0.002	nd		2.5E-06	3	4.7	4022	988	376	4	362	4	1.07	0.04	1.20	0.05	30.3	0.3	2.2	0.1	1.7	1.2
	95.4	cr #2	0.7	10.2	0.2	2.5	0.2	0.040	0.006	0.11	0.03	nd		10	3696	1379	318	2	313	2	1.67	0.06	1.89	0.09	6.7	0.1	2.7	0.3	7.8	1.4
	95.4	cr #3	0.6	9.5	0.2	1.8	0.1	0.024	0.002	0.07	0.04	7.1E-06	9	0.8	4160	1035	478	16	449	15	1.30	0.06	2.70	0.15	69.1	2.3	2.2	0.1	0.7	1.2
H3042-1 (dupl.)	36.3	cr #1	1.5	9.3	0.2	2.2	0.1	0.027	0.005	0.18	0.05	nd		5.0	3891	1837	371	13	357	13	0.98	0.05	1.06	0.08	29.2	1.0	2.1	0.4	1.8	1.1
P-Patch deposit - Quartz																															
P48-2	98.2	cr #1	1.6	9.5	0.2	2.6	0.1	0.032	0.001	0.12	0.01	1.6E-05	20	8.2	2460	275	318	1	307	1	1.02	0.04	1.39	0.06	19.7	0.1	0.6	0.1	2.6	0.3
	98.2	cr #2	1.5	9.5	0.2	2.7	0.1	0.031	0.001	0.12	0.01	4.8E-05	58	5.7	2660	384	329	2	315	2	1.02	0.04	1.10	0.05	26.2	0.2	0.7	0.1	1.9	0.4
	98.2	cr #3	1.7	9.5	0.2	2.6	0.1	0.031	0.001	0.10	0.02	2.7E-05	33	4.7	2689	556	343	6	324	5	1.06	0.04	1.08	0.06	36.0	0.7	0.8	0.1	1.4	0.4
	98.2	cr #4	2.1	9.0	0.2	2.5	0.1	0.032	0.001	0.11	0.01	5.4E-05	66	5.8	2395	299	335	2	315	2	1.02	0.04	1.12	0.06	36.5	0.4	0.5	0.1	1.4	0.3
	98.2	cr #5	2.3	9.1	0.2	2.5	0.1	0.029	0.001	0.08	0.01	1.4E-04	169	4.1	2773	289	370	3	341	3	1.00	0.05	1.34	0.13	56.8	0.7	0.8	0.05	0.9	0.4
P48-5	107.5	cr #1	6.0	8.7	0.1	2.9	0.1	0.028	0.001	0.09	0.01	4.1E-06	5	23	3075	226	337	1	324	1	1.07	0.04	1.15	0.05	26.9	0.1	1.1	0.04	1.7	0.5
	107.5	cr #2	2.6	8.5	0.2	2.8	0.1	0.027	0.001	0.08	0.01	4.3E-06	5	5.9	3004	245	360	2	339	2	1.11	0.04	1.37	0.06	44.9	0.4	1.0	0.03	1.0	0.5
	107.5	cr #3	2.2	8.3	0.2	2.8	0.1	0.027	0.001	0.08	0.01	7.7E-06	8	3.8	2866	336	371	3	343	3	1.09	0.04	1.63	0.09	57.1	0.6	0.8	0.04	0.8	0.4
	107.5	cr #4	2.4	8.1	0.2	2.2	0.0	0.029	0.001	0.08	0.01	9.4E-06	10	2.8	3154	221	440	4	396	3	1.16	0.04	1.43	0.11	85.7	0.9	1.2	0.03	0.5	0.6
McArthur River deposit - Quartz																															
MAC54Qz	103.2	cr #1	1.2	6.6	0.1	8.2	0.2	0.041	0.001	0.13	0.03	2.6E-05	29	8.0	2229	373	314	2	303	2	1.01	0.04	1.33	0.06	15.0	0.1	0.5	0.1	3.1	0.2
	103.2	cr #2	0.9	6.3	0.1	6.7	0.2	0.041	0.001	0.09	0.02	2.9E-05	33	4.7	2193	324	318	2	304	2	1.02	0.04	1.34	0.07	18.4	0.2	0.5	0.1	2.5	0.2
	103.2	cr #3	1.4	6.4	0.1	6.0	0.2	0.045	0.002	0.10	0.01	5.5E-05	61	4.9	1778	432	323	5	300	4	1.02	0.04	1.31	0.07	29.3	0.5	0.1	0.1	1.6	0.1
	103.2	cr #4	0.6	6.3	0.1	4.6	0.2	0.044	0.002	0.13	0.03	8.6E-05	96	1.6	1655	337	327	5	297	4	1.04	0.04	1.33	0.11	38.6	0.6	0.04	0.1	1.2	0.02
Rabbit Lake deposit - Quartz																															
RBL2Qz	95.5	cr #1	0.5	6.0	0.1	5.6	0.2	0.048	0.006	0.10	0.06	nd		2.7	2185	463	319	1	305	2	1.04	0.04	1.14	0.10	16.7	0.1	0.6	0.04	3.0	0.3
	95.5	cr #2	0.6	5.9	0.1	5.1	0.1	0.056	0.002	0.11	0.03	nd		4.8	2344	765	320	5	307	5	1.03	0.04	1.14	0.05	13.2	0.2	0.9	0.4	3.8	0.4
	95.5	cr #3	0.9	5.8	0.1	4.8	0.1	0.054	0.002	0.10	0.01	nd		3.0	2073	377	338	5	310	5	1.09	0.04	1.46	0.07	29.6	0.5	0.5	0.1	1.7	0.2
RBL7Qz	91.6	cr #1	0.6	8.3	0.1	3.1	0.1	0.033	0.005	0.09	0.05	1.6E-05	19	1.7	1778	584	320	4	299	5	0.97	0.04	1.02	0.04	35.7	0.5	0.1	0.1	1.4	0.1
	91.6	cr #2	0.5	8.4	0.2	3.0	0.1	0.034	0.005	0.06	0.04	3.5E-05	41	0.9	1719	946	332	17	299	16	0.97	0.07	1.17	0.16	54.2	2.7	0.1	0.3	0.9	0.04
	91.6	cr #3	0.3	8.1	0.2	2.9	0.1	0.037	0.002	0.19	0.06	1.0E-04	118	0.4	630	225	309	4	263	5	0.86	0.05	1.88	0.15	69.4	0.8	*		0.7	*
Rabbit Lake deposit - Dolomite																															
RBL2Carb	132	cr #1	0.4	7.8	0.1	4.8	0.4	0.047	0.004	nd		6.4E-05	72	16	3260	1267	304	2	301	2	1.00	0.07	1.15	0.04	2.7	0.1	2.2	0.5	17.3	1.0
	132	cr #2	0.6	8.0	0.3	3.8	0.3	0.046	0.007	nd		3.7E-05	42	11	2561	2995	304	12	300	12	1.01	0.05	1.19	0.06	5.0	0.2	1.0	2.5	9.5	0.5
	132	cr #3	0.3	7.9	0.2	4.0	0.1	0.035	0.004	nd		3.5E-05	39	4.2	2989	936	310	2	305	2	1.02	0.04	1.31	0.07	7.8	0.1	1.2	0.2	6.0	0.6
RBL7Carb	101.4	cr #1	2.5	8.8	0.2	3.3	0.1	0.027	0.001	nd		1.8E-05	21	25	2487	509	306	1	301	1	1.01	0.04	1.18	0.05	10.2	0.1	0.5	0.1	4.7	0.3
	101.4	cr #2	1.0	8.7	0.2	2.8	0.1	0.029	0.001	nd		7.5E-05	86	4.7	1178	184	302	1	292	1	0.96	0.07	1.12	0.06	20.9	0.2	*		2.3	*
	101.4	cr #3	0.5	8.4	0.2	3.0	0.1	0.017	0.005	nd		1.3E-04	148	2.0	2994	1627	319	4	311	5	0.97	0.04	1.23	0.19	26.8	0.4	0.6	0.1	1.8	0.3

Table 3

Sample name	Sample weight (mg)	Cl mol g^{-1} ($\times 10^{-6}$)	Br/Cl ($\times 10^{-3}$)	±	I/Cl ($\times 10^{-6}$)	±	K/Cl	±	U/Cl	^{36}Ar mol g^{-1} ($\times 10^{-14}$)	Age Ma	±	^{40}Ar/^{36}Ar Measured	±	^{40}Ar/^{36}Ar (1.6 Ga)	±	F(^{84}Kr/^{36}Ar)$_{air}$	±	F(^{129}Xe/^{36}Ar)$_{air}$	±
Eagle Point deposit - Quartz																				
ES287-10	38.6	0.8	5.7	0.1	7.2	1.5	6.46	0.11	2.2E-03	6.3	1376	28	1543	4	*		1.57	0.12	51.56	2.16
H3042-1	31.8	0.7	6.6	0.1	4.4	0.8	0.28	0.03	1.8E-03	7.6	**		291	5	246	12	1.46	0.12	20.93	1.13
P-Patch deposit - Quartz																				
P48-2	93.9	3.0	6.5	0.1	3.9	0.4	0.45	0.01	1.2E-02	38.8	961	84	326	1	264	2	1.51	0.20	2.77	0.08
McArthur River deposit - Quartz																				
MAC54Qz	95.7	2.4	5.0	0.04	5.1	0.3	0.28	0.01	1.3E-02	26.0	817	124	314	1	268	2	1.97	0.26	2.59	0.07
Rabbit Lake deposit - Quartz																				
RBL2Qz	72.5	0.8	4.4	0.04	4.5	0.2	0.76	2.01	4.7E-04	6.7	993	175	374	4	221	8	1.86	0.11	14.26	0.61
	33.1	2.2	4.9	0.04	4.1	0.2	0.23	10.32	1.2E-04	14.2	831	438	322	4	258	12	0.92	0.06	2.90	0.19

Figure 1

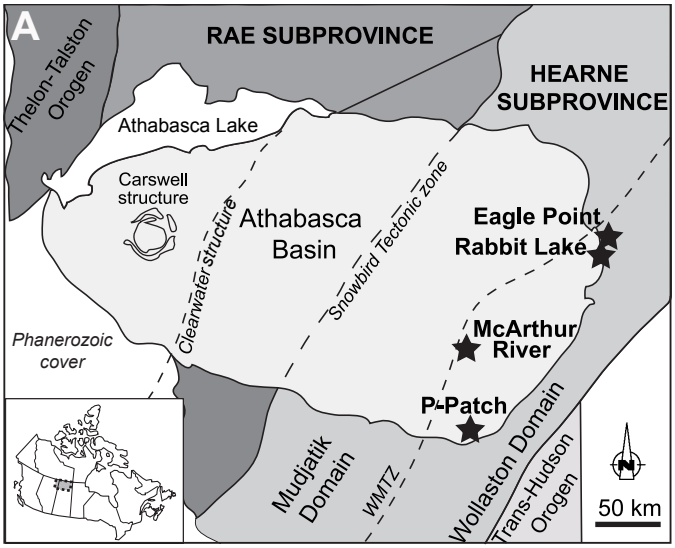
A
RAE SUBPROVINCE
HEARNE SUBPROVINCE
Thelon-Talston Orogen
Athabasca Lake
Carswell structure
Athabasca Basin
Clearwater structure
Snowbird Tectonic zone
Eagle Point
Rabbit Lake
McArthur River
P-Patch
Phanerozoic cover
Mudjatik Domain
WMTZ
Wollaston Domain
Trans-Hudson Orogen
50 km

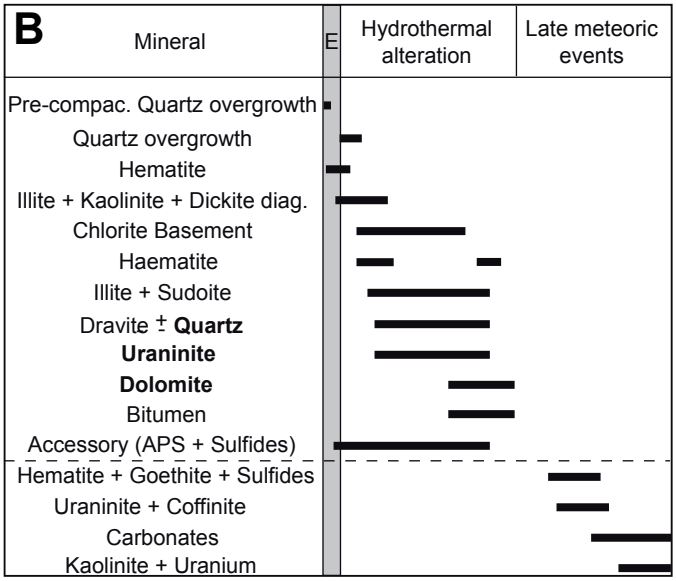
B
Mineral
E
Hydrothermal alteration
Late meteoric events
Pre-compac. Quartz overgrowth
Quartz overgrowth
Hematite
Illite + Kaolinite + Dickite diag.
Chlorite Basement
Haematite
Illite + Sudoite
Dravite ± Quartz
Uraninite
Dolomite
Bitumen
Accessory (APS + Sulfides)
Hematite + Goethite + Sulfides
Uraninite + Coffinite
Carbonates
Kaolinite + Uranium

Figure 2

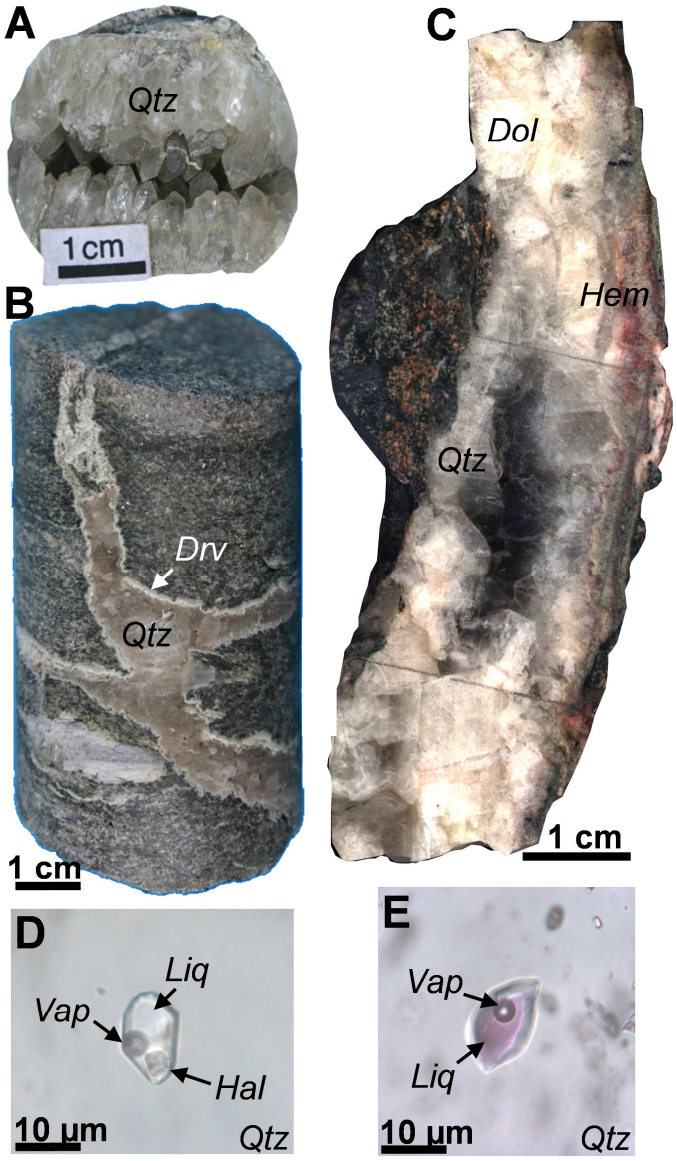
A
Qtz
1 cm
B
Drv
Qtz
1 cm
C
Dol
Hem
Qtz
1 cm
D
Liq
Vap
Hal
10 µm
Qtz
E
Vap
Liq
10 µm
Qtz

Figure 3

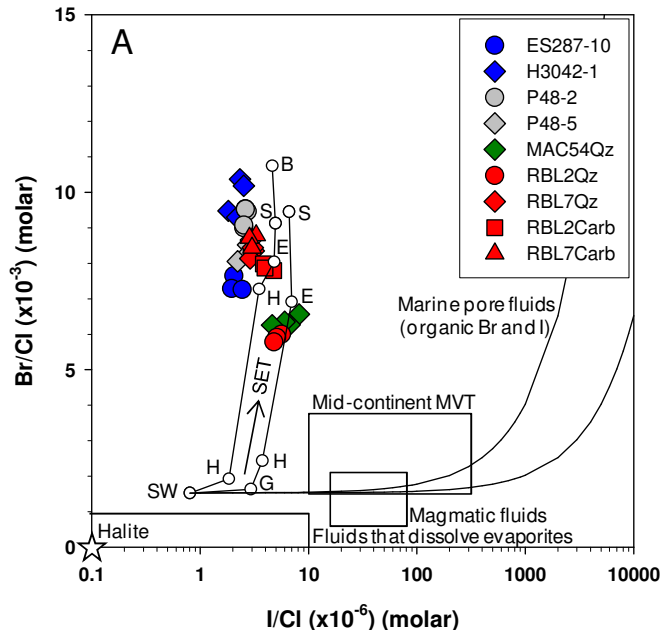
A
ES287-10
H3042-1
P48-2
P48-5
MAC54Qz
RBL2Qz
RBL7Qz
RBL2Carb
RBL7Carb
Marine pore fluids
(organic Br and I)
Mid-continent MVT
Magmatic fluids
Fluids that dissolve evaporites
Halite
SET
SW
B
S
E
H
G
Br/Cl (x10-3) (molar)
I/Cl (x10-6) (molar)
0.1
1
10
100
1000
10000

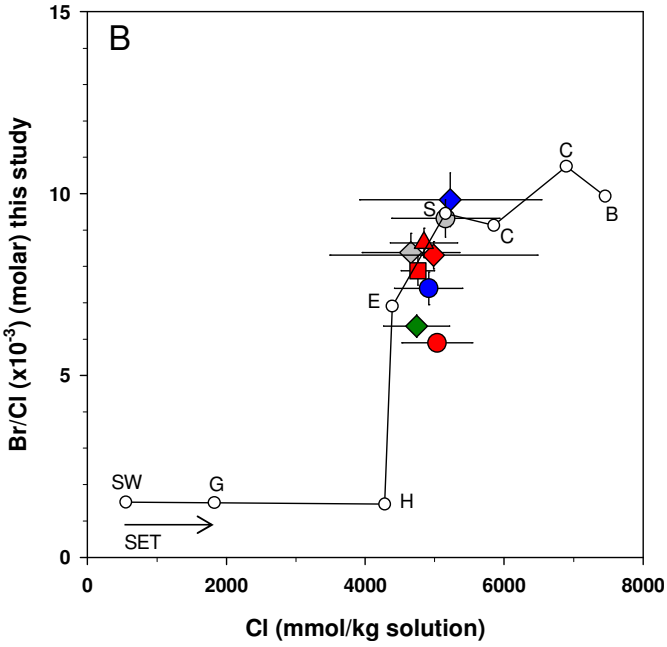
B
Br/Cl (x10-3) (molar) this study
Cl (mmol/kg solution)
SW
G
H
SET
C
S
E
B
0
2000
4000
6000
8000

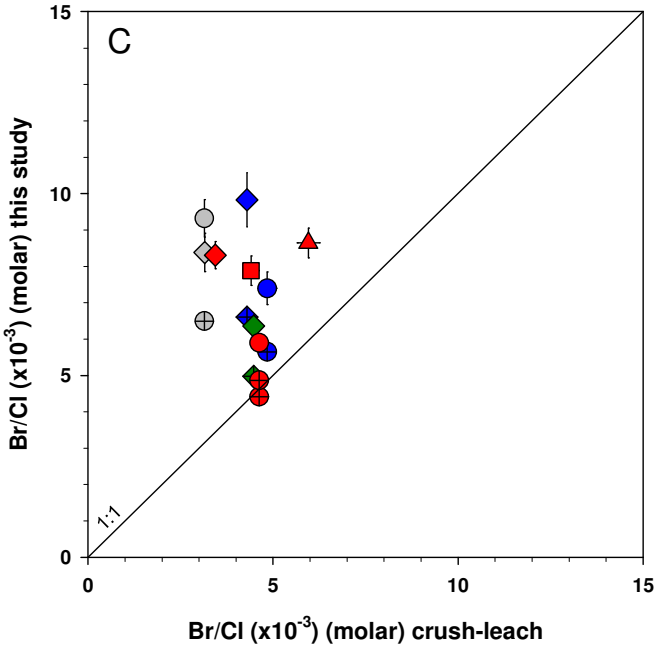
C
Br/Cl (x10-3) (molar) this study
Br/Cl (x10-3) (molar) crush-leach
1:1
0
5
10
15

Figure 4

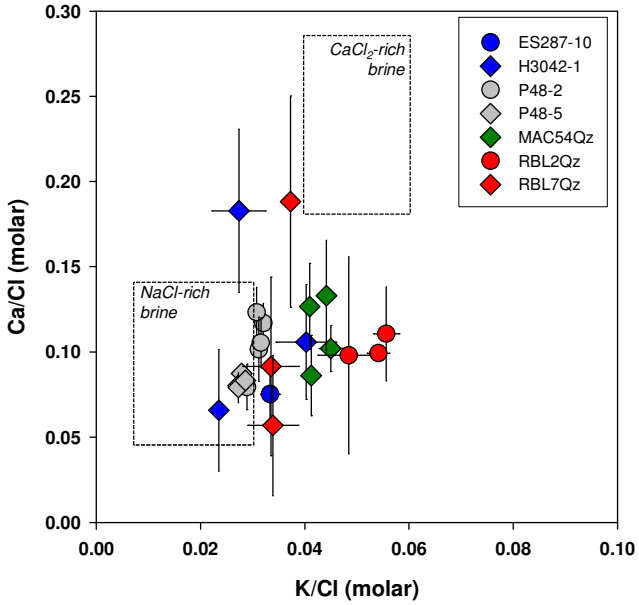
0.30
0.25
0.20
0.15
0.10
0.05
0.00
Ca/Cl (molar)
0.00
0.02
0.04
0.06
0.08
0.10
K/Cl (molar)
CaCl2-rich brine
NaCl-rich brine
ES287-10
H3042-1
P48-2
P48-5
MAC54Qz
RBL2Qz
RBL7Qz

Figure 5

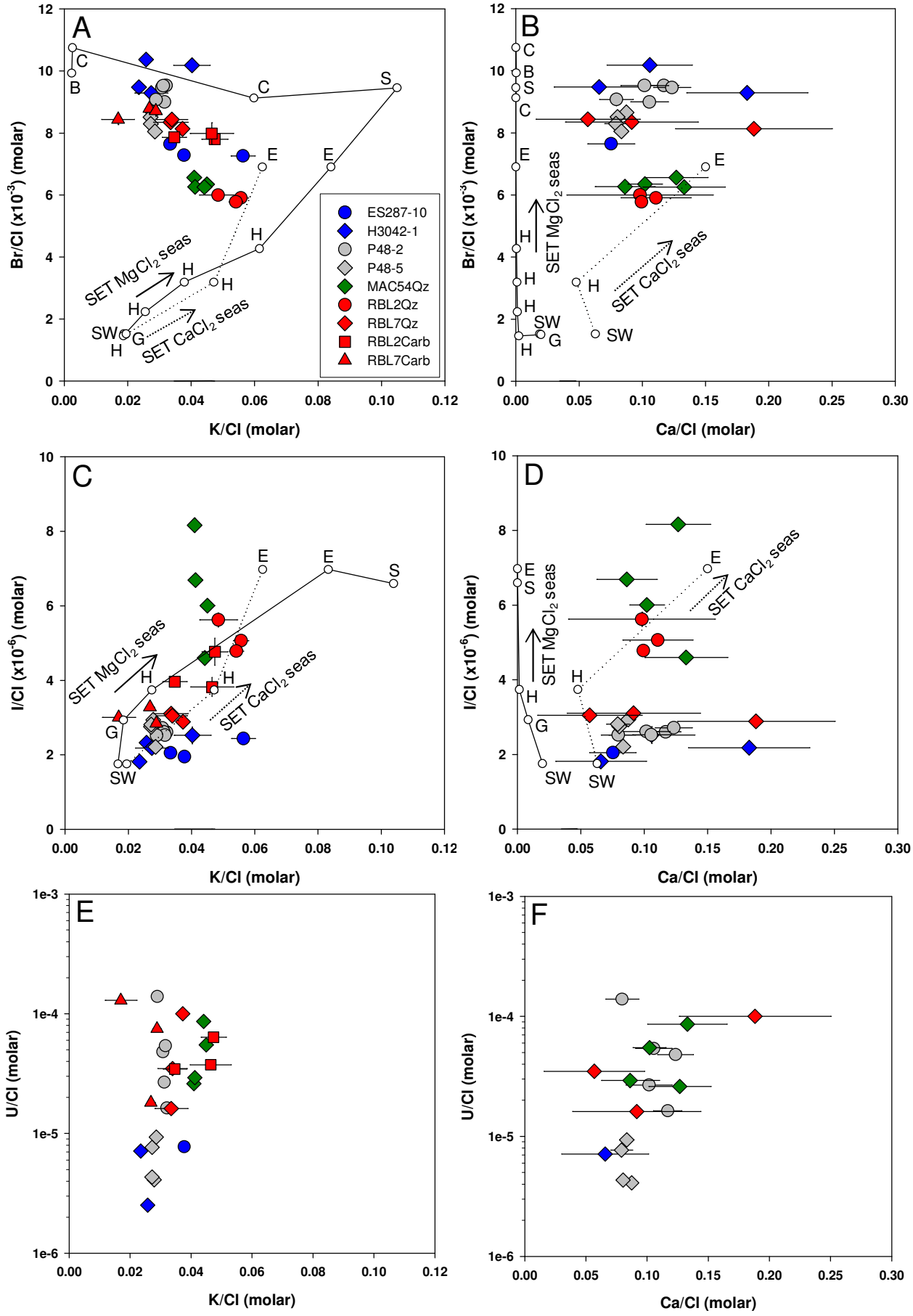
A
B
C
D
E
F
Br/Cl (x10^{-3}) (molar)
I/Cl (x10^{-6}) (molar)
U/Cl (molar)
K/Cl (molar)
Ca/Cl (molar)
ES287-10
H3042-1
P48-2
P48-5
MAC54Qz
RBL2Qz
RBL7Qz
RBL2Carb
RBL7Carb
SET MgCl$_2$ seas
SET CaCl$_2$ seas
C
B
S
E
H
SW
G

Figure 6

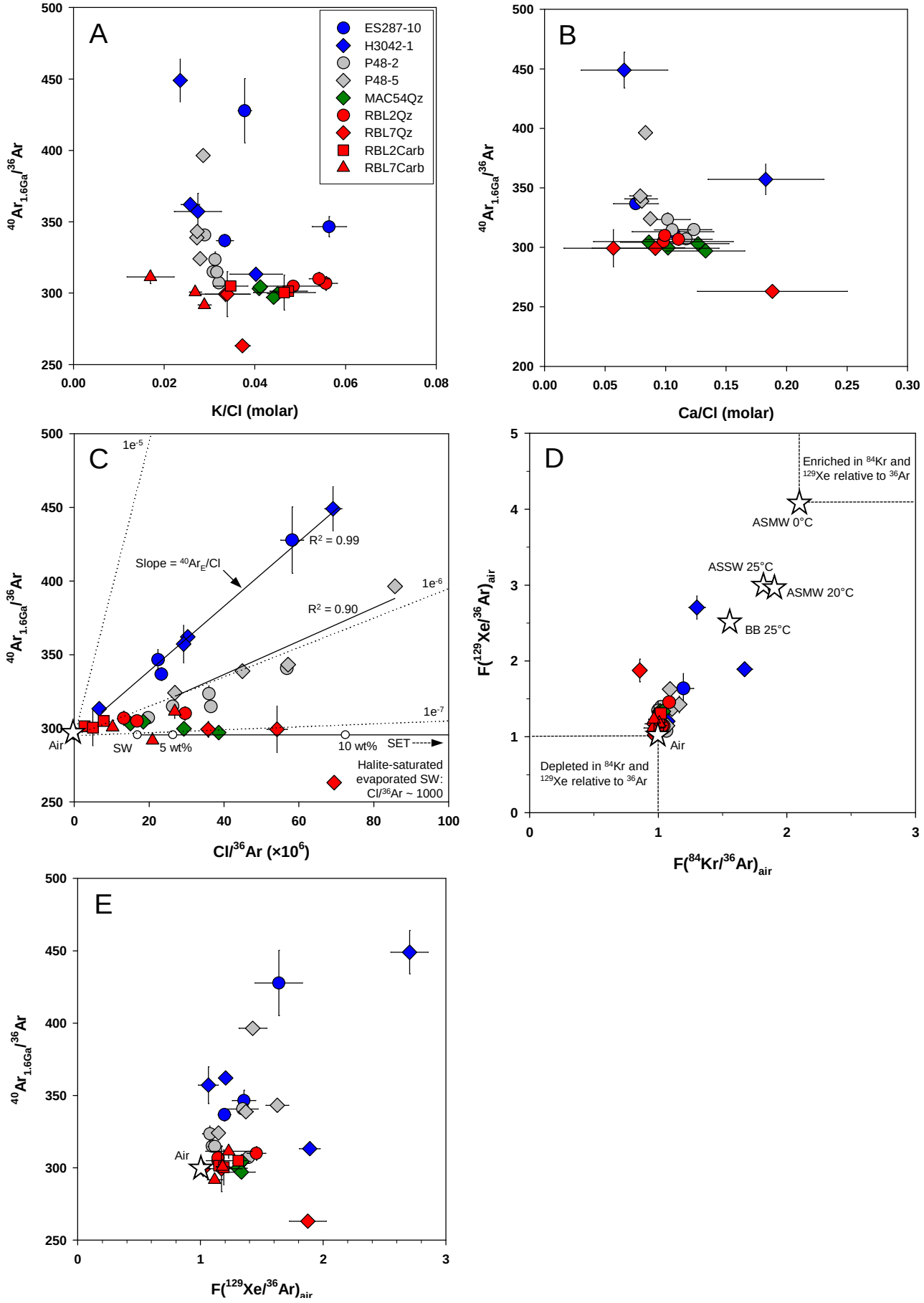
A
ES287-10
H3042-1
P48-2
P48-5
MAC54Qz
RBL2Qz
RBL7Qz
RBL2Carb
RBL7Carb
$^{40}Ar_{1.6Ga}/^{36}Ar$
K/Cl (molar)
B
Ca/Cl (molar)
C
1e-5
1e-6
1e-7
Slope = $^{40}Ar_E/Cl$
R^2 = 0.99
R^2 = 0.90
Air
SW
5 wt%
10 wt%
SET
Halite-saturated evaporated SW: $Cl/^{36}Ar$ ~ 1000
$Cl/^{36}Ar$ (×10^6)
D
Enriched in ^{84}Kr and ^{129}Xe relative to ^{36}Ar
ASMW 0°C
ASSW 25°C
ASMW 20°C
BB 25°C
Air
Depleted in ^{84}Kr and ^{129}Xe relative to ^{36}Ar
$F(^{129}Xe/^{36}Ar)_{air}$
$F(^{84}Kr/^{36}Ar)_{air}$
E
Air
$F(^{129}Xe/^{36}Ar)_{air}$